*Article*

# Study on Combustion Characteristics and NOx Formation in 600 MW Coal-Fired Boiler Based on Numerical Simulation

**Bo Zhu [1], Bichen Shang [2,*], Xiao Guo [1], Chao Wu [1], Xiaoqiang Chen [3] and Lingling Zhao [2]**

[1] Huanggang Dabieshan Power Generation Co., Ltd., Macheng 438300, China
[2] School of Energy and Environment, Southeast University, Nanjing 210096, China
[3] Zhongdian Huachuang Electric Power Technology Research Co., Ltd., Suzhou 215124, China
\* Correspondence: bichen_shang@163.com

**Abstract:** The variations in the boiler operation conditions have a great effect on the combustion characteristics and the pollutant formation in furnaces. This work aims to investigate the effects of operational parameters on NOx formation and its distribution in furnaces using the numerical simulation method to obtain the optimum control strategy for reducing NOx emissions. The numerical simulation models of pulverized coal combustion in furnaces involving flow, heat transfer, combustion and NOx formation are established. Taking a 600 MW supercritical opposed firing pulverized coal boiler as the study object, a full-scale three-dimensional physical model of the boiler is constructed with Gambit software. On this basis, the pulverized coal combustion and the NOx formation under various boiler loads are numerically simulated using the software of Ansys Fluent 2021R1, and the accuracy and the reliability of the models established are verified by comparing the simulation data with the field test data. According to the combustion numerical simulation of 128 groups of operating conditions, the effects of boiler load, the air rate and the air temperature on combustion and NOx formation have been emphatically investigated. The simulation results indicate that the formation of NOx and the NOx concentration distribution are mainly affected by the oxygen concentration and the temperature in the furnace. Especially, the effects of the variation in the excess air coefficient, the over-fire air (OFA) ratio, the primary air ratio and the internal secondary air ratio on NOx concentration distribution vary greatly. When the air temperature increases the overall NOx concentration in the furnace increases, and the influence of the secondary air temperature and the OFA temperature is greater than that of the primary air temperature. Large amounts of simulation data are a necessary data source for further study on the NOx prediction model at the economizer outlet, which can improve the prediction ability and the generalization ability of the NOx prediction model.

**Keywords:** combustion characteristics; NOx formation; numerical simulation; coal-fired boiler

## 1. Introduction

A clean and low-carbon energy system taking renewable energy as the mainstay are being built in China in order to address the increasingly pressing issues of energy security, environmental degradation, climate warming, etc. However, the instability of the power grid frequency is gradually increasing because of the increase in generating capacity from the renewable energy generator sets. The coal-fired generating units play a key role in the peak modulation and the frequency modulation in the power grid to maintain the stability of the grid frequency. The operating conditions of the power plant boilers vary frequently with the constant adjustment of the boiler load. The changes in the boiler operating conditions have a great effect on the combustion in the furnace and the NOx concentration in the economizer outlet. It has been reported that the fluctuation amplitude of the NOx concentration at the economizer outlet reached $\pm150$ mg/Nm$^3$ when the boiler load was adjusted for a 600 MW supercritical pressure generating unit. It brings great

difficulty to the regulation of the ammonia injection of SCR denitrification facility, which usually results in excessive ammonia injected into the SCR denitrification facility for the environmental protection [1,2]. Therefore, the ammonia escape increases sharply because of excessive ammonia injected, which can lead to serious problems such as ash deposition and heavy clogging because of the ammonium bisulfate formed in the air heater. Finally, it seriously affects the economic efficiency and the environmental protection performance of the power generation sets. The main reason for the aforementioned problems is that there is a large hysteresis during the adjustment of the amount of ammonia injected according to the measured value of NOx concentration at the exit of the SCR reactor. In recent years, some researchers have proposed to establish a prediction model of NOx concentration at the economizer outlet according to the operational parameters, and the variation in the NOx concentration at the economizer outlet can be predicted when the operating conditions begin to change, so as to coordinate the adjustment of ammonia injection and make timely operational adjustments. This idea has been generally recognized, and the prediction model about NOx is considered to be an effective means to guide the ammonia injection of the SCR denitrification facility [3]. It is much too complicated to establish the prediction model of NOx, because its input parameters of the prediction model are directly related to the factors affecting the furnace combustion, such as the coal consumption, the air distribution, the oxygen content, etc. The parameter variation will influence the formation and the reduction in NOx in the furnace and further the NOx concentration at the economizer outlet. Under the background of deep peak shaving, the temperature and the oxygen amount in the furnace have greater influence on NOx formation [4]. Hence, it is necessary to investigate the influence factors and the laws of NOx formation in the furnace.

Scholars all around the world have performed a lot of research on the formation law of NOx and its prediction models. Generally, the data from the field tests and the distributed control system (DCS) of the power plant are used to establish the prediction models of NOx formation [5]. However, those data may fluctuate greatly and include many outliers, and as a result the data cleaning becomes a challenge for the modeling process. When the NOx concentration at the furnace outlet is taken as a mean value, without the consideration of the nonuniform NOx distribution on the cross section of the flue, it is unable to control the SCR denitrification facility to implement the partitioned ammonia injection. Fortunately, the numerical simulation based on the computational fluid dynamics (CFD) software can be used not only to analyze the influence law of various parameters on the NOx formation, but also to provide the detailed data for establishing the NOx prediction model [5].

At present, it is accepted that the NOx formation mechanism in coal combustion includes the thermal NOx, the prompt NOx and the fuel NOx [6–9]. The simple chemical model established by Zeldovich is generally used to describe the formation mechanism of thermal NOx [10]. The chemical reaction model established by De S is used to describe the formation mechanism of the fuel NOx [5,11]. The nitrogen component from the fuel is divided into the nitrogen fixed in char and the volatile nitrogen [12]. The volatile N is first released in the form of HCN and $NH_3$ during the pyrolysis process, then these substances are competitively oxidized to NO or reduced to $N_2$ according to the local oxidizing or reducing atmosphere [11]. However, the fixed N in char can be directly oxidized into NO. This formation model of fuel NOx is widely used in the simulation calculation. The prompt NOx is mainly produced by the hydrocarbons in the volatile matter of pulverized coal reacting with $N_2$ in air at high temperature. The prompt NOx accounts for a very small proportion of the total NOx [13], so the thermal NOx and the fuel NOx are usually mainly considered in many studies on the NOx formation in coal combustion [5,14–18].

In recent years, the domestic and foreign scholars have established the calculation models of NOx using CFD software and constantly optimized the models. In 2015, Fortunato et al. performed a numerical investigation into the roles of closure sub-models for the modelling of a flameless furnace and the main NO formation paths using the commercial software of Ansys Fluent 6.3 [19]. The results show that different combustion/kinetic models used can result in different distributions of temperature/chemical species in the

furnace and the $N_2O$ mechanism is the dominant factor influencing NO formation, but the formation mechanism of thermal NO is not as relevant as in traditional combustion regime. In 2016, Li et al. developed a new NOx calculation model for pulverized coal combustion by User-Defined Function (UDF) [20]. The gasification reaction models of char with $CO_2$ and $H_2O$ were added to the char combustion model during the developing of the NOx calculation model. Thus, the homogeneous reaction of NOx reduced by the hydrocarbons was quantitatively described through calculating the amount of CO and $H_2$ produced. In 2017, Tan et al. simulated the NOx formation process in a 660 MW tangentially fired boiler using the post-processing method [21], where the proportion of nitrogen in volatiles and char was determined by the chemical percolation devolatilization (CPD) model [22,23]. Their study results indicated that the NOx calculation results were more reasonable when the gasification reactions of char with $CO_2$ and $H_2O$ were considered in the char combustion reaction model. Thus, the relative error between the simulated value and the measured value is only 5.9%. Zhang et al. studied a circulating fluid bed boiler using the software of CFD and the chemical reactors(CR), and reasonably made use of the advantages of the total package reaction and the elementary reaction; ultimately, the accurate calculation results were obtained in the case of using less computing resources [24]. In 2022, Lamioni et al. investigated the effect of $H_2$ addition on the combustion process and the pollutant emissions in domestic condensing boilers through the coupling research between numerical simulations and the practical operating conditions [25]. The study results can help design the strategies to restrict pollutant emissions. The above research shows that the numerical simulation can be used to investigate the NOx formation in furnace combustion more effectively.

In recent years, some researchers have applied the intelligence algorithm to predict the generation of NOx. Meanwhile, other scholars are continually optimizing the NOx prediction algorithm and utilizing the NOx prediction model to optimize the boiler operation. The input parameters of the NOx prediction model are usually from the field tests and the DCS of the power plant [26]. The quality of the data will directly affect the training of the prediction model, and then determine the prediction accuracy of NOx generation. More detailed information on furnaces can be obtained by means of the numerical simulation based on the CFD software. The detailed information is not only used to investigate the influence law of many factors on the NOx formation, but also to be the new data source for the NOx prediction model. In 2019, Shi et al. established an artificial neural network (ANN) model for predicting the boiler operation and the NOx emission characteristics according to the simulated data and the boiler operational data [27]. The model provided a good prediction of the thermal efficiency and the NOx emission of a 660 MW coal-fired boiler, and the average errors were only 0.04% and 3.56 mg/$Nm^3$, respectively. The study results indicated that the CFD numerical simulation data contributed to the generalization ability of the neural network models. Ye et al. built the prediction model of NOx generation for a coal-fired power plant based on the historical operating data from the DCS and the numerical simulation data of the NOx [28]. The study results indicated the simulation data could improve the prediction ability of the model as well as the depth and the completeness of the data set.

Nowadays, the numerical simulation method has been relatively mature enough to obtain the combustion characteristics of the pulverized coal and the laws of NOx generation. However, the range of the previous simulation research is usually only from the burner inlet to the super-heater outlet. There is little system-wide research from the burner inlet to the economizer outlet, and the number of simulated operating conditions is also relatively small. Although the NOx emission can be predicted well via the machine learning method, the previous study is often only focused on describing the nonlinear relationships between the NOx concentration at the furnace outlet and the boiler operating parameters, without taking into consideration of other factors affecting the formation and reduction process of NOx. In addition, the prediction model established is unable to control the SCR denitrification facility to perform the partitioned ammonia injection if there is no consideration of

nonuniform NOx distribution on the cross section of flue. Under the background of the deep peak shaving, it is necessary to perform the simulation research on batch variable operating conditions; the detailed information from the numerical simulation can be a new data source of the prediction models of NOx formation, so that the prediction models can be further optimized to accurately guide the SCR denitrification facility achieving the partition ammonia injection.

In this study, taking a 600 MW supercritical opposed firing coal-fired boiler as the research object, the numerical calculation models of pulverized coal combustion and NOx formation are established. The numerical simulation of variable operational conditions is performed. The factors influencing NOx formation and its concentration distribution in the furnace are studied.

## 2. Models and Methods of Numerical Simulation

In this section, the numerical simulation models of combustion in the furnace including flow, heat transfer and pulverized coal combustion are established based on the literature [29]. The basic situation of a 600 MW supercritical swirl-opposed firing pulverized coal boiler is introduced, and its three-dimensional physical model from the burner to the economizer outlet is established according to the ratio of 1:1 [30]. The pulverized coal combustion process in the furnace under the base operational condition is numerically simulated using the software of Ansys Fluent 2021R1, and the simulation data are compared with the field experimental data to verify the accuracy and the reliability of the calculation models and the calculation methods. The physical and mathematical models established in this section can provide the basis for the subsequent variable condition calculations.

### 2.1. Numerical Simulation Models

The combustion process of pulverized coal in the boiler mainly includes the flow process of fluids and the combustion process of pulverized coal, which involves the processes of the volatile release, the gas phase combustion and the char combustion, and also involves the radiation heat transfer and the formation of pollutants. Therefore, it is more complicated to numerically simulate the combustion of pulverized coal in the boiler [31]. The mathematical models for the numerical simulation of furnace combustion are established. The numerical calculation methods and models are as follows.

#### 2.1.1. Basic Control Equations

The basic governing equations include the mass conservation equation, the momentum conservation equation and the energy conservation equation. The mass conservation equation is shown in Equation (1), which is suitable for the compressible and incompressible flows:

$$\frac{\partial \rho}{\partial t} + \nabla \cdot \left( \rho \vec{v} \right) = S_m \tag{1}$$

Here, $\rho$—the flue gas density, kg/m$^3$; $\vec{v}$—the velocity vector, m/s; $t$—time, s; $S_m$ is added to the mass of the continuous phase from a dispersed second phase (e.g., due to the droplet evaporation) and a user-defined mass source.

The momentum conservation equation is shown in Equation (2):

$$\frac{\partial \rho}{\partial t} \left( \rho \vec{v} \right) + \nabla \cdot \left( \rho \vec{v} \vec{v} \right) = -\nabla p + \nabla (\vec{t}) + \rho \vec{g} + \vec{F} \tag{2}$$

In Equation (2), $p$—the hydrostatic pressure, Pa; $\vec{t}$—the stress tensor, Pa; $\rho \vec{g}$—the gravity, N; $\vec{F}$—the outside force, N.

The energy conservation equation is shown in Equation (3):

$$\frac{\partial}{\partial t}(\rho h) + \frac{\partial}{\partial x_j}(\rho u_j h) = -p \frac{\partial u_j}{\partial x_j} + \frac{\partial}{\partial x_j} \left( \lambda \frac{\partial T}{\partial x_j} \right) + \Phi + S_h \tag{3}$$

Here, $x_j$—the displacement of the fluid in the j direction, m; $u_j$—the fluid velocity of the fluid in the j direction, m/s; $h$—the distance of fluid to the boundary, m; $T$—the thermodynamic temperature, K. $\frac{\partial}{\partial x_i}\left(\lambda \frac{\partial T}{\partial x_j}\right)$—the heat conduction term; $S_h$—heat source; $\Phi$—the dissipation term of the fluid mechanical energy.

### 2.1.2. Gas-Phase Turbulence Models

Generally, the gas flow in the boiler is in a strong disturbance state, so it is suitable to use the turbulent flow equations to solve the movement process of the gas flow in the furnace. In the gas-phase turbulence models, compared with the standard *k-ε* model and the RNG *k-ε* model, the Realizable *k-ε* model is more suitable for the fluid flow including the strong streamline curvature flow, the vortex flow and the swirl flow [15,18,32]. Therefore, the Realizable *k-ε* model with Wall Function is used to simulate and calculate the gas-phase turbulence in this study. The Realizable *k-ε* model includes k-equation and *ε*-equation, as shown in Equations (4) and (5):

$$\frac{\partial}{\partial t}(pk) + \frac{\partial}{\partial x_j}(\rho k u_j) = -\frac{\partial}{\partial x_j}\left[\left(\mu + \frac{\mu_t}{\sigma_k}\right)\frac{\partial k}{\partial x_j}\right] + G_k + G_b - \rho\varepsilon - Y_M + S_k \tag{4}$$

$$\frac{\partial}{\partial t}(\rho\varepsilon) + \frac{\partial}{\partial x_j}(\rho\varepsilon u_j) = -\frac{\partial}{\partial x_j}\left[\left(\mu + \frac{\mu_t}{\sigma_\varepsilon}\right)\frac{\partial\varepsilon}{\partial x_j}\right] + \rho C_1 S\varepsilon - \rho C_2 \frac{\varepsilon^2}{K + \sqrt{v\varepsilon}} + C_{1\varepsilon}\frac{\varepsilon}{k}C_{3\varepsilon}C_b + S_\varepsilon \tag{5}$$

Here, $k$—the turbulence pulsation kinetic-energy, J; $\varepsilon$—the dissipation rate of turbulence pulsation kinetic-energy,%; $\mu$—the turbulent viscosity of the fluid in the standard state, kg/(m·s); $\mu_t$—the turbulent viscosity of the fluid at a temperature ($t$), kg/(m·s); $\sigma_k$, $\sigma_\varepsilon$—the Prandtl constant of $k$ and $\varepsilon$, respectively; $G_k$—the turbulent kinetic energy due to the laminar velocity gradient, m$^2$/s$^2$; $G_b$—the turbulent kinetic energy due to the buoyancy, m$^2$/s$^2$; $Y_M$—the contribution of fluctuation expansion in the compressible turbulence to the total dissipation rate, m$^2$/s$^2$; $S_k$, $S_\varepsilon$—the user-defined source terms; $C_1$, $C_2$, $C_{1\varepsilon}$, $C_{3\varepsilon}$—the constant, respectively.

### 2.1.3. Gas-Solid Two-Phase Flow Models

The flow of pulverized coal and the gas in the boiler is a gas-solid two-phase flow, so a discrete phase model is used to describe the mixed flow [33] in which the gas is treated as continuous phase and the pulverized coal particles are treated as discrete phase. In this study, the incident pulverized-coal is defined as the incident particle. The Discrete Random Walk Model based on the Lagrange model is used to describe the motion process of the incident particles [34]. The interaction of particles with the turbulent vortices in the fluid phase is simulated using this model in this study. The velocity fluctuation of each vortex obeys the Gaussian probability distribution, as follows:

$$u' = \xi\sqrt{u'^2} \tag{6}$$

In Equation (6), the letter $\xi$ denotes a random number obeying a normal distribution. The remainder of $\xi\sqrt{u'^2}$ is a local random value of the velocity fluctuation. The crossing time ($t_{cross}$) of a particle through a vortex is defined as follows.

$$t_{cross} = -\tau \ln\left[1 - \left(\frac{L_e}{\tau|u - u_p|}\right)\right] \tag{7}$$

In Equation (7), the letter $\tau$ is the particle relaxation time and the sign $L_e$ is the vortex length scale. The absolute value $|u - u_p|$ represents the magnitude of the relative velocity.

2.1.4. Pulverized Coal Combustion Models

The combustion process of the pulverized coal is more complex, generally including the moisture evaporation, the volatiles devolatilization, the volatiles combustion and the char oxidation. Firstly, the volatile matter is released and catches fire during the heating process. Then the residual volatiles are released when the char is ignited and burns. Finally, the volatiles also burn out when the char burns out to form ash. The above processes affect each other and proceed simultaneously. Therefore, in the numerical simulation the different mathematical models are used to describe the devolatilization process, the volatiles combustion process and the char combustion process in the combustion process. In this study, the Probability Density Function (PDF) model is used to numerically simulate the species transportation during the combustion process of the pulverized coal.

Devolatilization Models

When the temperature is from 120–450 °C, the volatiles matter in coal can be released. In this study, the Two Competing Rates Model is employed to simulate the release process of the volatiles. The release rate of the volatiles is defined as follows:

$$-\frac{dm_p}{dt} = k[m_p - (1 - f_{v,0})m_{p,0}]$$ (8)

$$k = Ae^{-(E/RT)}$$ (9)

Here, $m_p$—the particle mass, kg; $f_{v,0}$—the initial mass fraction of the volatiles in particles; $k$—the kinetic rate, s$^{-1}$; $E$—activation energy, J/mol; $A$—the preexponential factor; $R$—the molar gas constant.

Assuming that the kinetic rates of the volatile release at low temperature and high temperature are $\Re_1$ and $\Re_2$, respectively, the two kinetic rates are weighted and brought into Equation (8) and thus the release rate of volatile matter $m_v$ (t) of the volatiles can be defined as follows:

$$\frac{m_v(t)}{m_{p,0} - m_a} = \int_0^t (\alpha_1\Re_1 + \alpha_2\Re_2) \exp\left(-\int_0^t (\Re_1 + \Re_2)dt\right) dt$$ (10)

In Equation (10), the letters $\alpha_1$ and $\alpha_2$ denote the yield factor, respectively. The symbol $m_a$ denotes the ash content in the particles and its unit is kilogram (kg).

Gas-Phase Combustion Models

The pulverized coal combustion is a typical non-premixed combustion. Consequentially, the non-premixed combustion model is suitable for the numerical simulation calculation of the pulverized coal combustion [4]. The pulverized coal combustion is simplified into a mixing problem based on the non-premixed combustion model, which avoids the difficulty in calculating the nonlinear average reaction rate. In this model, the substance involved in the thermochemical reactions is simplified into a parameter, namely the mixture fraction (f). This parameter is derived from the mass fraction of the elements of the fuel flow. The number of atoms in a substance is conserved in the chemical reactions, so the mixture fraction is a conserved scalar, the governing transport equation of which has no source term.

The basis of the non-premixed combustion modeling method is that the instantaneous thermochemical state of the fluid is related to the conservation scalar of the mixture fraction. The mixture fraction can be expressed by the atomic mass fraction, as follows:

$$f = \frac{Z_i - Z_{i,ox}}{Z_{i,fuel} - Z_{i,ox}}$$ (11)

In Equation (11), the symbol $Z_i$ is the mass fraction of the element $i$., and the subscripts *ox* and *fuel* represent the oxidant and the fuel at the inlet, respectively.

Assuming that the diffusivity is the same, the composition equation can be simplified to a single equation about the mixture fraction. The time-averaged mixture fraction equation is expressed as below:

$$\frac{\partial}{\partial t}\left(\rho\overline{f}\right) + \nabla \cdot \left(\rho\overrightarrow{v}\overline{f}\right) = \nabla \cdot \left(\left(\frac{k'}{C_p} + \frac{\mu_t}{\sigma_t}\right)\right) + S_m + S_{user} \tag{12}$$

In Equation (12), $\overline{f}$—the average value of the mixture fraction. $k'$—the laminar thermal conductivity of the mixture, W/(m·K). $C_p$—the specific heat capacity of the mixture, J/(kg·K); $\sigma_t$—the Prandtl constant; $S_m$—the mass term of the pulverized coal particles passed into the gas phase; $S_{user}$—the user-defined source term.

Char Combustion Models

The char combustion is a heterogeneous chemical reaction, which is described using the kinetic-diffusion control reaction rate models in this study. The effects of diffusion and reaction kinetics on the particle surface reaction rate are taken into account in the models.

The expressions of the oxygen diffusion rate $(D_0)$ to the char surface and the chemical reaction kinetic rate$(R)$ on the char surface are as follows, respectively:

$$D_0 = C_1\frac{\left(\left(T_p + T_\infty\right)/2\right)^{0.75}}{d_p} \tag{13}$$

$$R = C_2e^{-(E/RT_p)} \tag{14}$$

Here, $T_p$ and $T_\infty$ denote the Kelvin temperature of the reactant surface and the Kelvin temperature of the surrounding medium, respectively. The symbol $d_p$ is the surface area of the chemical reaction, the unit of which is square meter. $C_1$ and $C_2$ separately represent the diffusion rate constant and the chemical reaction rate constant.

The surface reaction combustion rate $(\frac{dm_p}{dt})$ of char is obtained by weighting the diffusion rate and the chemical reaction rate, as below:

$$\frac{dm_p}{dt} = -\pi d_p^2 p_{ox}\frac{D_0R}{D_0 + R} \tag{15}$$

In Equation (15), this symbol of $p_{ox}$ indicates the partial pressure of the gaseous oxidant around the particles and its unit is Pa. This letter $R$ is the kinetic reaction constant considering the reaction and the diffusion on the inner surface of char.

According to the mass fraction of the oxidant, and assuming that the particle size is constant and the particle density decreases, the reaction combustion rate $(\frac{dm_p}{dt})$ on the char surface can be obtained as shown in Equation (16):

$$\frac{dm_p}{dt} = -\pi d_p^2\frac{\rho RT_\infty Y_{ox}}{M_{w,ox}}\frac{D_0R}{D_0 + R} \tag{16}$$

Here, $Y_{ox}$—the mass fraction of oxidant in the local gas; $M_{w,ox}$—the molar mass of oxidant, g/mol.

2.1.5. Radiation Heat Transfer Models

Radiation heat transfer is the main way of heat transfer in the furnace, which accounts for about 90% of the total heat transfer. In this study, the $P_1$ model is used to simulate the radiation heat transfer. The radiant heat flux $q_r$ of the model is expressed as Equation (17):

$$q_r = -\frac{1}{3(a + \sigma_s) - C\sigma_s}\nabla G \tag{17}$$

Here, $a$—the absorption coefficient; $\sigma_s$—the scattering coefficient; $G$—the incident radiation rate; $C$—the anisotropic phase function coefficient. The expression of the incident radiation rate $G$ is as shown in Equation (18):

$$\nabla \cdot (\Gamma \nabla G) - aG + 4an^2\sigma T^4 = S_G \tag{18}$$

In Equation (18), the letter $n$ represents the refractive index of the medium and the letter $\sigma$ is the Stefan–Boltzmann constant. The letter $a$ is same as the above definition. The letter $\Gamma$ is a parameter introduced to describe Equation (18), and its calculation formula is as below:

$$\Gamma = \frac{1}{3(a + \sigma_s) - C\sigma_s} \tag{19}$$

The spectral emissivity ($G_{b\lambda}$) between the wavelength of $\lambda_1$ and $\lambda_2$ is calculated as Equation (20):

$$G_{b\lambda} = 4[F(0 \rightarrow n\lambda_2)T - F(0 \rightarrow n\lambda_1)T]\sigma T^4 \tag{20}$$

In Equation (20), the symbol $F\ (0 \rightarrow n\lambda T)$ denotes the ratio of the radiation energy emitted by a blackbody in the wavelength range from 0 to $\lambda$ m.

### 2.1.6. NOx Formation Models

The NOx from the combustion in furnace is mainly the nitric oxide (NO), followed by the nitrogen dioxide ($NO_2$) and the nitrous oxide ($N_2O$). The formation of NOx can be attributed to four different chemical kinetics processes, including the thermal NOx formation, the prompt NOx formation, the fuel NOx formation and the intermediate $N_2O$ formation, among which the prompt NOx accounts for a very small proportion of the total NOx and is negligible [13,35,36]. The convection, the diffusion, the generation and the depletion among NOx and the related substances have been taken into account during solving the mass transfer equation of NOx. For the thermal NOx and the prompt NOx, only the mass transport equation of NO is needed, as shown in Equation (21):

$$\frac{\partial}{\partial t}(\rho Y_{NO}) + \nabla\left(\rho \vec{v} Y_{NO}\right) = \nabla \cdot (\rho \Im \nabla Y_{NO}) + S_{NO} \tag{21}$$

Here, the symbol of $Y_{NO}$ denotes the mass fraction of NO in the gas phase. The symbol of $\Im$ represents the effective diffusion coefficient.

The formation mechanism of the fuel NOx is more complex, and it is necessary to solve the transport equations of NO, HCN, $NH_3$ and $N_2O$, which are shown as Equations (21)–(24), respectively:

$$\frac{\partial}{\partial t}(\rho Y_{HCN}) + \nabla\left(\rho \vec{v} Y_{HCN}\right) = \nabla \cdot (\rho \Im Y_{HCN}) + S_{HCN} \tag{22}$$

$$\frac{\partial}{\partial t}(\rho Y_{NH_3}) + \nabla\left(\rho \vec{v} Y_{NH_3}\right) = \nabla \cdot \left(\rho \Im Y_{NH_3}\right) + S_{NH_3} \tag{23}$$

$$\frac{\partial}{\partial t}(\rho Y_{N_2O}) + \nabla\left(\rho \vec{v} Y_{N_2O}\right) = \nabla \cdot \left(\rho \Im Y_{N_2O}\right) + S_{N_2O} \tag{24}$$

Here, $Y_{HNC}$, $Y_{NH3}$ and $Y_{N2O}$ are the mass fractions of HNC, $NH_3$ and $N_2O$, respectively. For the different formation mechanisms of NOx, the source terms of $S_{HNC}$, $S_{NH3}$, $S_{N2O}$ and $S_{NO}$ are also different.

#### Reaction Formation Models of Thermal NOx

The thermal NOx formation is determined by a set of highly temperature-dependent chemical reactions that is called the extended Zeldovich mechanism [37–40]. This model is used to simulate the thermal NOx formation. The molecules of $N_2$ in the air are oxidized

by the oxygen atoms forming the thermal NOx when the reaction temperature is over 1800 K [41]. The main governing reactions of thermal NOx are as follows:

$$O + N_2 \rightleftharpoons N + NO \tag{25}$$

$$N + O_2 \rightleftharpoons O + NO \tag{26}$$

$$N + OH \rightleftharpoons H + NO \tag{27}$$

In the three reactions mentioned above, the forward reaction rate is expressed as $k_{f,1}$, $k_{f,2}$ and $k_{f,3}$, respectively, and the backward reaction rate as $k_{r,1}$, $k_{r,2}$ and $k_{r,3}$, respectively.

In reaction (R1) there is a very high activation energy required to break three strong chemical bonds in $N_2$ in order that O atoms react with N atoms to form NO. Therefore, the chemical reaction obviously occurs only at a high temperature above 1800 K, which is the rate-limiting step of the Zeldovich mechanism [37–41]. However, in reaction (R2) the activation energy required for the oxidation of N atoms is very small and the depletion rate of free N atoms is equal to its formation rate when oxygen gas ($O_2$) is sufficient. Consequentially, the quasi-steady state form of the NO formation rate can be established, as shown in Equation (25):

$$\frac{d[NO]}{dt} = 2k_{f,1}[O][N_2] \frac{\left(1 - \frac{k_{r,1}k_{r,2}[NO]^2}{k_{f,1}[N_2]k_{f,2}[O_2]}\right)}{\left(\frac{k_{r,1}[NO]}{k_{f,2}[O_2] + k_{f,3}[OH]}\right)} \tag{28}$$

The formation of NOx in the above reactions is greatly affected by the temperature. When the temperature is above 2200 K, the formation rate of thermal NOx will double with the increase of 90 K in temperature. To solve Equation (25), in addition to the stable concentration of substances (i.e., $O_2$ and $N_2$) the concentrations of O atom and OH radicals are determined based on the partial equilibrium assumption [17,42]. At present, the equilibrium method, the partial equilibrium method and the predictive concentration method are used to predict the concentration of O atom. Among them, the equilibrium method separates the formation mechanism of thermal NOx from the main combustion process by assuming the equilibrium values of the temperature, the stable matter, the O atoms and the OH radicals.

Reaction Formation Models of Fuel NOx

Generally, fuel NOx is considered as the important source of NOx formation in large-scale pulverized coal furnaces [35,40]. The N in the fuel NOx comes from the volatile matter and the N in char [35,43]. Since the N proportion in the two substances is unknown, it is necessary to assume its proportion for the further calculation. The conversion of the fuel N into NOx depends on the local combustion characteristics and the initial concentration of the nitrogen compounds. These compounds are thermally decomposed in the reaction zone to form the free radicals such as HCN, $NH_3$, N, CN and NH, and then converted into NOx. The above radicals have undergone a double competition reaction pathway. Although the pathways leading to the formation and the destruction of the fuel NOx are still not fully clear [40], the currently accepted simplified model is shown in Figure 1, that is, the nitrogen-containing intermediate compounds will be competitively oxidized to NO or reduced to $N_2$ according to the local atmosphere [11]. In this study, the global model established by De Soete [11] is employed to describe the fuel NOx formation.
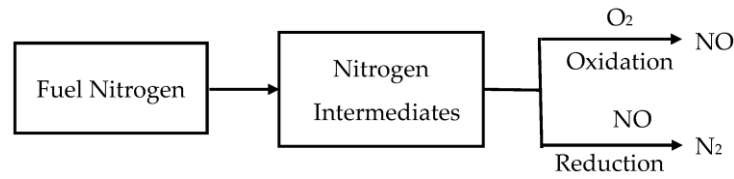
**Figure 1.** A simplified model of fuel NOx formation pathway.

When HCN is the intermediate product, the source terms in the transport Equations (21) and (22) can be written as below:

$$S_{NO} = S_{NO-1} + S_{NO-2} \tag{29}$$

$$S_{HCN} = S_{pl,HCN} + S_{HCN-1} + S_{HCN-2} \tag{30}$$

Here, the symbols $S_{NO-1}$ and $S_{NO-2}$ represent the effects of HCN being oxidized or reduced on NO. The symbols $S_{NO}$ and $S_{HCN}$ denote the changes in NO and HCN. The symbols $S_{HCN-1}$ and $S_{HCN-2}$ denote the effects of HCN being oxidized or reduced on HCN. The symbol $S_{pl,HCN}$ denotes the effects of the fuel combustion on HCN.

For the gas fuel, the formation rate of HCN is equivalent to the combustion rate of fuel. For the liquid fuel, the rate at which HCN is formed is equivalent to the fuel evaporation rate into the gas phase. For gas and liquid fuels the consumption rates of HCN are the same. When the fuel is gaseous and liquid the conversion rates of HCN are separately represented using $R_1$ and $R_2$, the formulas of which are as below:

$$R_1 = A_1 X_{HCN} X_{O_2}^a e^{-E_1/RT} \tag{31}$$

$$R_2 = A_2 X_{HCN} X_{NO}^a e^{-E_2/RT} \tag{32}$$

Here, the unit of $R_1$ and $R_2$ is s$^{-1}$ and X is mole fraction.

When NH$_3$ is the intermediate product, the source terms in the transport Equations (21) and (22) can be expressed as below:

$$S_{NO} = S_{NO-1} + S_{NO-2} \tag{33}$$

$$S_{NH_3} = S_{pl,NH_3} + S_{NH_3-1} + S_{NH_3-2} \tag{34}$$

Here, the symbols $S_{NO-1}$ and $S_{NO-2}$ represent the effects of NH$_3$ being oxidized or reduced on NO. The symbols $S_{NO}$ and $S_{NH_3}$ denote the changes in NO and NH$_3$. The symbols $S_{NH_3-1}$ and $S_{NH_3-2}$ denote the effects of NH$_3$ being oxidized or reduced on NH$_3$. The symbol $S_{pl,NH_3}$ denotes the effects of the fuel combustion on NH$_3$.

For the gas fuel, the formation rate of NH$_3$ is equivalent to the combustion rate of fuel. For the liquid fuel, the rate at which NH$_3$ is formed is equivalent to the fuel evaporation rate into the gas phase. For the gas fuel and the liquid fuel the consumption rates of NH$_3$ are the same. When the fuel is gaseous and liquid the conversion rates of NH$_3$ are separately represented using $R_3$ and $R_4$, the formulas of which are as below:

$$R_3 = A_3 X_{NH_3} X_{O_2}^a e^{-E_3/RT} \tag{35}$$

$$R_4 = A_4 X_{NH_3} X_{NO}^a e^{-E_4/RT} \tag{36}$$

Here, the unit of $R_3$ and $R_4$ is s$^{-1}$.

When the fuel is solid, both HCN and NH$_3$ can be formed as reactive intermediates at sufficiently high temperature. For brown coal, the production of NH$_3$ is 10 times that of HCN while the production of HCN is 9 times that of NH$_3$ for the bituminous coal. Therefore, the proportion of the fuel converted into HCN and NH$_3$ can be assigned in order to simulate and calculate the NOx formation more expediently.

Reaction Formation Models of Prompt NOx

The proportion of the prompt NOx in the total NOx is smaller, and it is mainly generated in the early stage of combustion. A series of complex reactions and many possible intermediates can occur during the generation of the prompt NOx. At present, the accepted reaction pathways can be described by reaction (R4)–(R7) [20]:

$$CH + N_2 \rightleftharpoons HCN + N \tag{37}$$

$$N + O_2 \rightleftharpoons NO + O \tag{38}$$

$$HCN + OH \rightleftharpoons CN + H_2O \tag{39}$$

$$CH + O_2 \rightleftharpoons NO + CO \tag{40}$$

### 2.2. Overview and Geometric Modeling of Boiler

#### 2.2.1. Boiler Overview

In this study, the research object is a supercritical coal-fired once-through boiler in a 600 MW power plant. The furnace is 21.94 m in width, 15.57 m in depth, and 63 m in height. Here, the height is the distance from the centerline of the lower header under the front and rear water walls to the centerline of the furnace roof tubes. The overall layout of the boiler heating surfaces and the burners is shown in Figure 2. The boiler is an opposed-firing boiler with swirl burners. The front and rear walls are equipped with three layers of low nitrogen swirl burners and one layer of low NOx dual air-adjusting nozzles (i.e., over fire air (OFA) nozzles). There are 6 burners in each layer. The distance between the burners in each layer is 5 m. The distance between the centerline of the top layer burners and the centerline of the OFA nozzles is 4.5 m. The distance between the centerline of the bottom layer burners and the dry bottom hopper is 2.8 m. The distance between each column burner is 3 m, and the distance between the outermost burners and the side wall is 3.272 m.
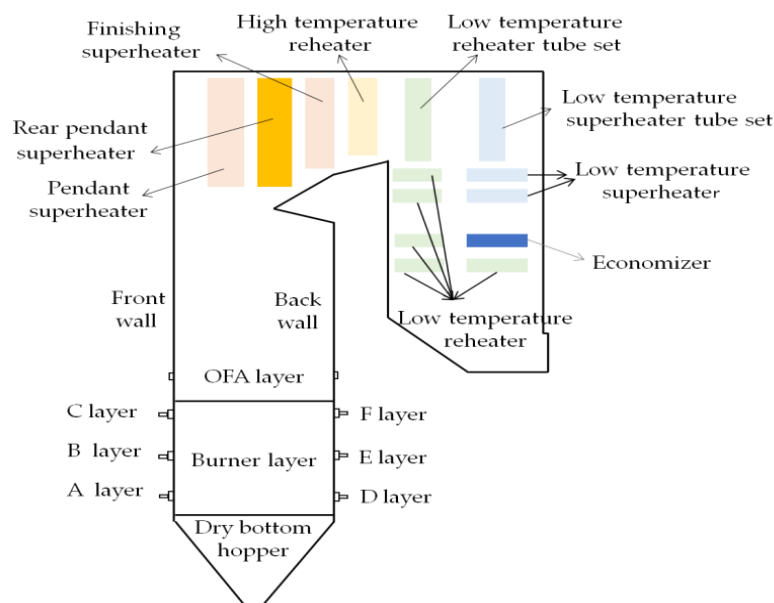


**Figure 2.** Boiler layout.

The direct-fired pulverizing system with HP-type medium-speed mill is used in the boiler. The boiler is equipped with six coal mills, each of which provides the pulverized coal to six burners on the same layer in the same wall. The air duct of the swirl burner (main burner) is divided into a central primary air duct and a two-layer swirl air duct on the outside. The unique flame stabilization device in the primary air duct makes the pulverized coal ignite violently as soon as the pulverized coal is ejected from the nozzle, thereby

strengthening the pyrolysis of the pulverized coal, maximizing the release of volatiles, and reducing the combustible part of carbon and the fuel nitrogen remaining in the ash particles. The swirl design of the inner and outer secondary air can effectively control the flame length and make the pulverized coal burn in stages. Due to the good reductive atmosphere at the outlet of the burner the fuel nitrogen is reduced to the nitrogen gas by a lot of hydrocarbons in the gas state, thereby reducing the formation of NOx. The OFA duct includes a central duct and an outer ring duct. The central wind is a direct current wind to maintain the stiffness of the inlet wind, and the outer ring duct is equipped with adjustable blades. The rotating airflow from the outer ring duct helps the secondary air of the OFA fully mix with the flue gas. The OFA can provide the necessary oxygen gas for the later combustion of pulverized coal to ensure the full burnout of pulverized coal particles and control the carbon content in fly ash.

### 2.2.2. Geometric Modeling and Grid Division Methods

Geometric modeling is the basis of simulation calculation. According to the actual structure and the size of the boiler a three-dimensional geometric model at a ratio of 1: 1 is established for the whole furnace, as shown in Figure 3. Because the structure of the furnace itself and the calculated boundary conditions have good symmetry, the symmetry surface can be set to Symmetry in this research, namely only a half of the furnace model is established. This method not only cannot make the calculation results produce error, but also can improve the calculation speed and save the computing time. The geometric model established includes the burner, the OFA nozzle, the water wall, the superheater, etc., as much as possible to present the actual structure of the boiler from the burner inlet to the economizer outlet.
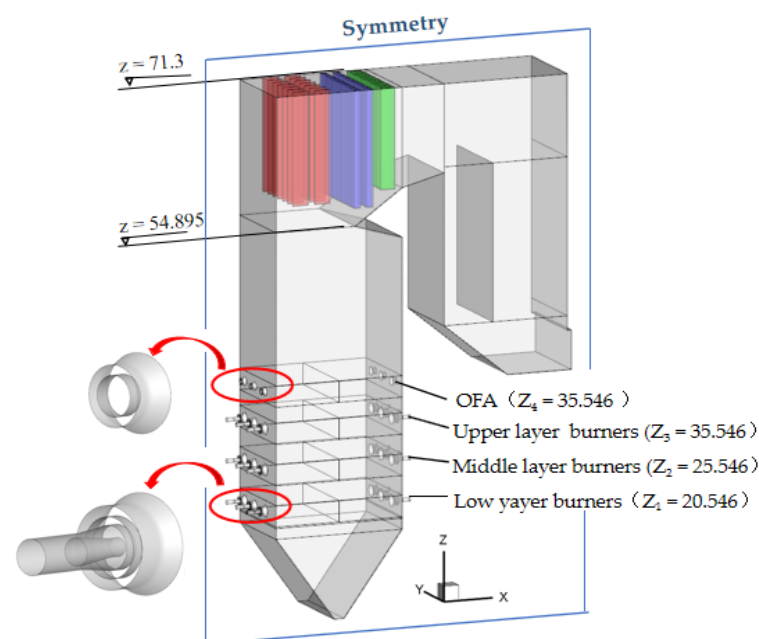


**Figure 3.** Three-dimensional geometric model of the boiler.

In order to obtain the data transfer from the burner to the furnace, the burner and the furnace in the model are set as a whole flow area. However, the structure of the swirl burner is complex and there are a large number of burners. In order to improve the calculation speed, the structure of the burner is simplified without affecting the simulation effect. The physical structure of the primary air pipe, the internal and external secondary air pipes, the central air pipe and the outer ring air pipe of the burner are simulated using the geometric structure of the circular table and the cylinder. In the simulation calculation, the inlet

boundary condition of the swirl flow is used to simulate the swirl flow of the internal and external secondary air of the burner and the outer ring air of the OFA.

The Gambit 2.4.6 software (ANSYS Fluent; Canonsburg; USA.) is used in this research. The structured grid is employed to divide the whole furnace as far as possible, and the divided grids are shown in Figure 4. It can be seen from Figure 4 that the structured grids are all utilized in the dry bottom hopper, the combustion zone in the furnace, the horizontal flue and the shaft flue area, and only a small number of unstructured grids are utilized around the burner and the superheater. Due to the violent combustion reaction in the combustion zone, the fluid disturbance and the temperature change are large. To ensure the calculation accuracy the refined grids are used in the combustion zone, but the sparse grids are used in the dry bottom hopper, the horizontal flue and the shaft flue so as to save the calculation resources and improve the calculation efficiency. During the meshing process, due to the small structure of the burner and the large structure of the furnace the grids at the interface will change greatly, which increases the difficulty of meshing. The interface between the burner and the furnace is set up by using the boundary conditions of the Interface in order to resolve the difficulty. Considering the influence of grid quantity on the calculation accuracy and the simulation speed, three meshing schemes have been performed in this study according to a method of a grid independent test [5,44]. The quantity of grid cells is 2.78 million, 3.82 million and 4.60 million, respectively. The main difference is that the grid cell quantity of the burner area is different. The temperature distribution obtained in the furnace height is basically similar using three meshing schemes. In order to ensure the calculation accuracy and decrease the calculating time, the grid cells 3.82 million has been utilized in this study.
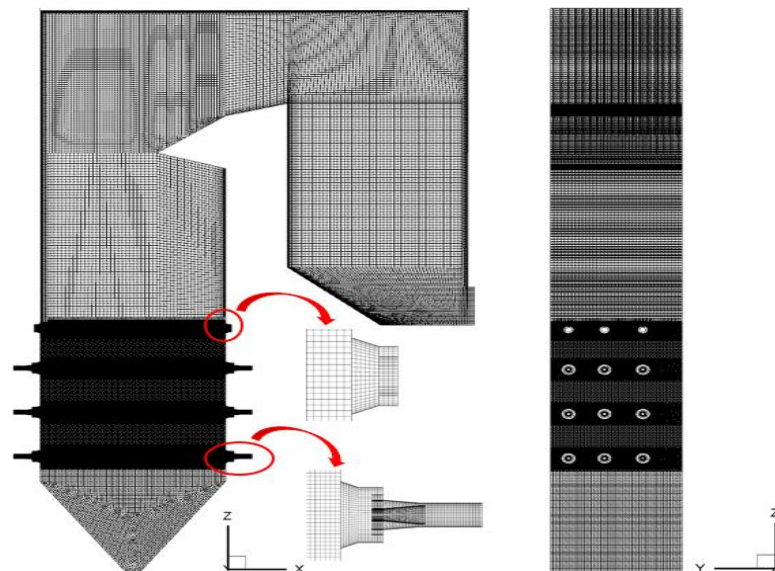


**Figure 4.** Grids formed in furnace.

*2.3. Validation and Analysis of Numerical Models*

2.3.1. Setting of the Base Operation Condition

To verify the reliability and the accuracy of the numerical models established, the simulation results of a certain operation condition need to be compared with the field measured data. In this study, the boiler maximum continuous rating (BMCR: 600 MW) is taken as the base operation condition. Meanwhile, six coal mills are put into operation. The main operating parameters of the base operation condition are listed in Table 1.

**Table 1.** Main operating parameters of the base operation condition (BMCR: 600 MW).

| Operating Parameter | Output of a Burner | Primary Air Rate | OFA Rate | Secondary Air Rate | Primary Air Temperature | Secondary Air Temperature |
|---|---|---|---|---|---|---|
| Units | kg/s | kg/s | kg/s | kg/s | K | K |
| value | 2.38 | 146.4 | 124.37 | 333 | 350 | 580 |

During the numerical simulation of the base operation condition, the air rate of burners in each layer is evenly distributed. The inner and the outer secondary air of the burners and the outer ring air of OFA are all set as the swirling flow at the inlet. The swirl intensity is obtained by adjusting the radial, axial and tangential velocities of the inlet air. The incident particles are used to simulate the pulverized coal particles into the furnace, the particle size distribution of which conforms to Rosin–Rammler distribution. In addition, the wall temperature, the emissivity of the furnace wall and the gas pipes are set according to the operating parameters.

The numerical simulation of the gas flow in boiler cold state is first performed. Then the combustion numerical simulation of the boiler is implemented at the burning temperature of 1800 K after the flow field calculation results converge. Finally, the simulation calculation of NOx formation is carried out by post-processing, and the calculation results of NOx are obtained.

2.3.2. Reliability Verification of Numerical Models

Some important simulation results are compared with the corresponding measured data, which are listed in Table 2. It can be seen from Table 2 that all the relative errors are less than 5%. In addition, the flow field, the temperature field and the species concentration field under the base operation condition have been analyzed according to the numerical simulation data. The simulation results have indicated that the numerical models and the calculation methods established in this study have high reliability and accuracy.

**Table 2.** Comparison between the numerical simulation results and the field measured data under the base operation condition.

| Items | Simulation Value | Measured Value | Relative Error |
|---|---|---|---|
| Flue gas temperature at the last-stage superheater outlet (K) | 1226 | 1249 | 1.80% |
| NOx concentration at the economizer outlet (mg/m$^3$) | 334 | 342 | 2.34% |
| Oxygen content at the economizer outlet (%) | 2.36 | 2.45 | 3.61% |
| Carbon content of fly ash at the economizer outlet (%) | 2.57 | 2.66 | 2.30% |

## 3. Results and Discussion

In this section the numerical calculations of the combustion process in the furnace under variable operating conditions are performed, based on the established physical and mathematical models. The effects of the boiler load, the air rate and the air temperature on the parameters, including the NOx concentration and the burnout rate of pulverized coal at the furnace outlet, have been analyzed to provide the data for the prediction of NOx concentration and more accurately guide the ammonia injection of the SCR denitrification facility.

### 3.1. Operating Condition Setting and Description of Batch Quantity Calculation

According to the range of peak regulation in the historical operation of the boiler, the boiler loads from 250 to 600 MW are selected as the research objects, and the combustion processes in the furnace under 8 different load conditions have been simulated. The specific operating parameters of 8 different conditions are listed in Table 3.

**Table 3.** Boiler operating parameters under 8 different boiler loads.

| Operating Condition | Boiler Load (MW) | Coal Mill in Operation | Single Burner Output (kg·s$^{-1}$) | Primary Air Rate (t/h) | Secondary Air Rate (t/h) | OFA Rate (t/h) | Primary Air Temperature (K) | Secondary Air Temperature (K) |
|---|---|---|---|---|---|---|---|---|
| 1 | 600 | ABCDEF | 2.39 | 527 | 1190 | 456.4 | 350 | 565 |
| 2 | 550 | ABCDEF | 2.19 | 486.9 | 1127 | 418.8 | 355.1 | 563.9 |
| 3 | 500 | ABCDE | 2.38 | 451.7 | 1072 | 385.8 | 251.3 | 561 |
| 4 | 450 | ABCDE | 2.15 | 416.3 | 1014 | 353 | 355.2 | 560.4 |
| 5 | 400 | ABCD | 2.38 | 373.3 | 932.1 | 314.2 | 345.3 | 559 |
| 6 | 350 | ABCD | 2.09 | 338.9 | 967.7 | 283 | 349.5 | 558.1 |
| 7 | 300 | ABCD | 1.79 | 303.4 | 796.7 | 251.4 | 348 | 557.6 |
| 8 | 250 | ABCD | 1.49 | 263.3 | 709 | 216.3 | 349.6 | 555.3 |

Based on the study of boiler load change, the influences of the air amount and the air temperature are researched under 4 boiler loads including 600, 500, 400 and 250 MW. The changed air amount conditions include the changed excess air coefficient, the changed OFA ratio, the changed primary air ratio and the changed internal secondary air ratio. The changed supply air temperature conditions include the changed primary air temperature and the changed temperature of the secondary air and the OFA. Each of the above parameters changes 20 working conditions, so there are a total of 120 groups of working conditions, as listed in Table 4. It should be noted that other parameters remain unchanged when studying the influences of a parameter change on the formation and the distribution of NOx.

**Table 4.** Conditions of variable air distribution rate and variable air distribution temperature.

| Base Conditions | Variable Parameters | | Setting Value | Condition Number |
|---|---|---|---|---|
| 600 MW 500 MW 400 MW 250 MW | air amount | excess air coefficient | 1.1, 1.2, 1.3, 1.4, 1.5 | 20 |
| | | OFA ratio | 15%, 20%, 25%, 30%, 35% | 20 |
| | | primary air ratio | 20%, 22.5%, 25%, 27.5%, 30% | 20 |
| | | secondary air ratio | 20%, 27.5%, 35%, 42.5%, 50% | 20 |
| | supply air temperature | primary air temperature | 335 K, 345 K, 355 K, 365 K, 375 K | 20 |
| | | secondary air temperature and OFA temperature | 550 K, 555 K, 560 K, 565 K, 570 K | 20 |

During the numerical simulation, the inlet boundary of the furnace model in this study includes the inlet boundary of 36 burners and 12 OFA nozzles. Each burner is equipped with a primary air inlet, an internal secondary air and an external secondary air inlet. When the working condition is changed more than 300 inlet parameters will change, which makes the operating process of setting the inlet parameters very complicated. Consequently, in this study the command statements for modifying the parameters are exported from the Journal file included in Fluent software, and the scripts are written in Python language, so that these statements can be read repeatedly by the solver of Fluent software. Additionally, the values required to be modified are automatically read according to the ID information of the model boundary surface, which greatly reduces human labor. Meanwhile, the command statements in the solver of Fluent software to calculate the sectional temperature, the NOx concentration, etc., are similarly processed.

### 3.2. Effects of Boiler Loads on NOx Formation

3.2.1. Effects on the Distributions of the Temperature Field and O$_2$ Concentration

When the boiler load is separately 600, 500, 400 and 250 MW, the temperature distribution on the central longitudinal section of the furnace burner is shown in Figure 5. It can be seen from Figure 5 that the temperature distribution in the furnace is basically the

same under different boiler loads and is well symmetrical. As the boiler load decreases the temperature of the furnace center decreases, and the high temperature zone of the furnace center gradually becomes smaller. When the boiler load is 600 MW, a large amount of pulverized coal is injected into the furnace from the upper burner and is not burnt out in the combustion zone. However, the unburned pulverized coal burns violently in the burning-out zone, which makes the temperature higher in the furnace upper zone and easily causes ash fouling on the superheater. When the boiler load is 500 MW there is no pulverized coal through the F-layer burners, but there is only a small amount of primary air and secondary air injected into the furnace. This ensures that the flame is still in the center of the furnace and prevents the flame deflection. When the boiler load is 250 MW, the temperature of the dry bottom hopper is also significantly reduced.



(**a**) (**b**) (**c**) (**d**)
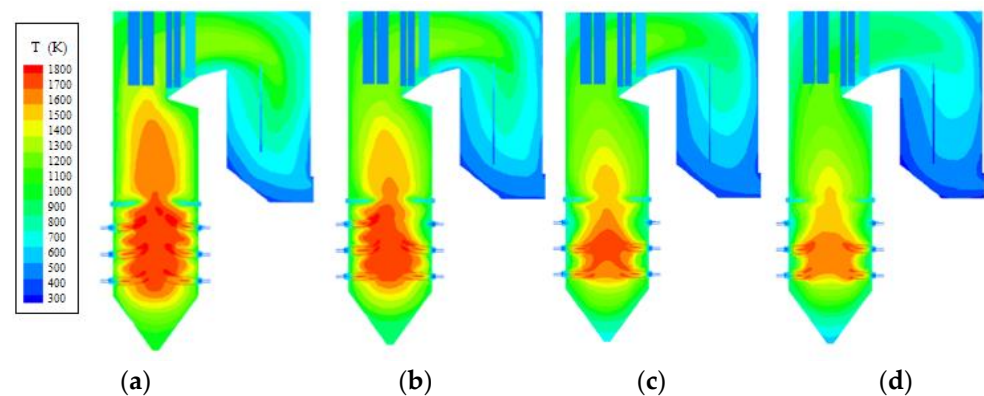
**Figure 5.** Temperature field distribution under different boiler loads: (**a**) Temperature field distribution under 600 MW boiler load; (**b**) Temperature field distribution under 500 MW boiler load; (**c**) Temperature field distribution under 400 MW boiler load; (**d**) Temperature field distribution under 250 MW boiler load.

In the actual operation of the power plant, the air–coal ratio is often larger under the lower boiler load. When the boiler load is separately 600, 500, 400 and 250 MW, the volume concentration of $O_2$ on the central longitudinal section of the furnace burners is shown in Figure 6. As shown in Figure 6, with the declining of the boiler load the overall $O_2$ concentration in the furnace increases. When the boiler load is 500 MW the $O_2$ concentration is higher because there is no pulverized coal through the F-layer burners. When the boiler load is 400 MW and below the upper burners are completely shut down, so the $O_2$ concentration in the area near the OFA is higher.



(**a**) (**b**) (**c**) (**d**)
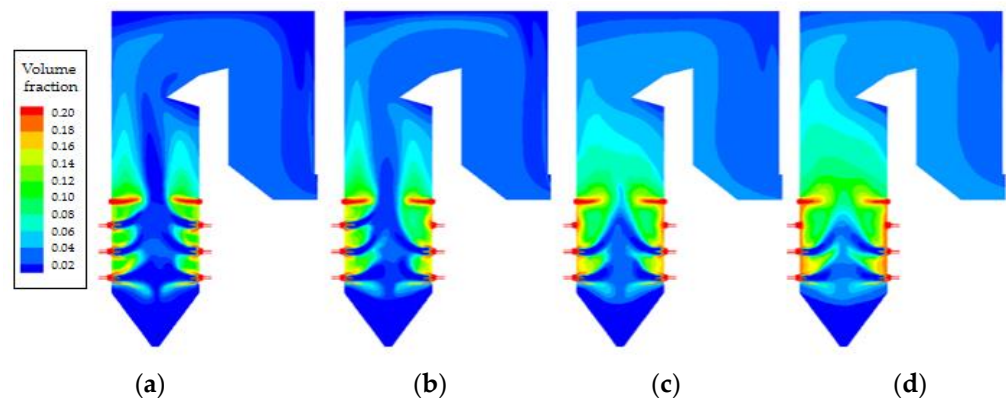
**Figure 6.** Distribution of $O_2$ volume concentration under different loads: (**a**) Distribution of $O_2$ volume concentration under 600 MW boiler load; (**b**) Distribution of $O_2$ volume concentration under 500 MW boiler load; (**c**) Distribution of $O_2$ volume concentration under 400 MW boiler load; (**d**) Distribution of $O_2$ volume concentration under 250 MW boiler load.

### 3.2.2. Effects on the Distribution of NOx Concentration

When the boiler load is separately 600, 500, 400 and 250 MW, the NOx concentration on the central longitudinal section of the furnace burner is shown in Figure 7. It can be seen that when the boiler load is reduced from 600 to 400 MW, the overall NOx concentration in the furnace is reduced. When the boiler load is 250 W the NOx concentration is the highest among them. When the boiler load is 600 MW the central temperature of the furnace is higher (see Figure 5a), and a large amount of thermal NOx is generated. When the boiler load declines, the furnace center temperature decreases (see Figure 5b–d) and the thermal NOx is greatly reduced. When the boiler load is 250 MW, due to the larger ratio of air to coal in the boiler at low boiler load the $O_2$ concentration in furnace is high, forming a strong oxidizing atmosphere and generating a large amount of fuel NOx, so the NOx concentration is greater.
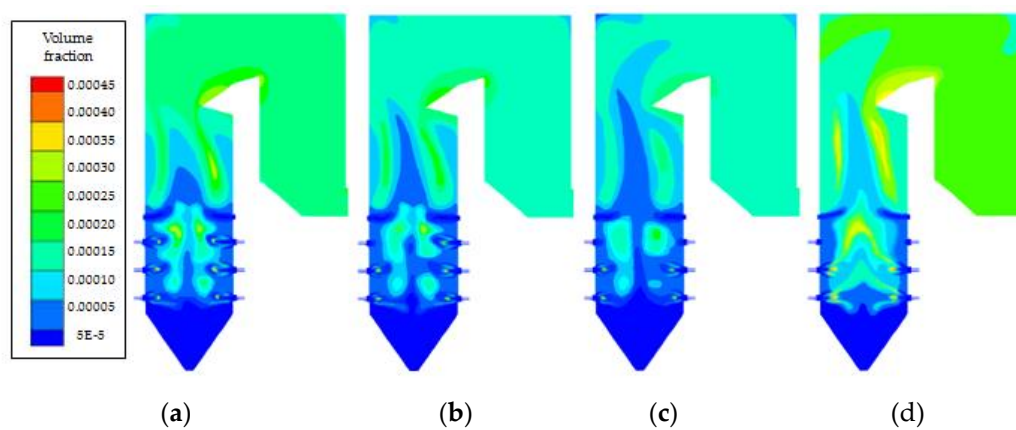


**Figure 7.** NOx concentration distribution under different loads: (**a**) NOx concentration distribution under 600 MW boiler load; (**b**) NOx concentration distribution under 500 MW boiler load; (**c**) NOx concentration distribution under 400 MW boiler load; (**d**) NOx concentration distribution under 250 MW boiler load.

Based on the above analysis, the NOx concentrations at the outlet plane of the economizer under different boiler loads are quantitatively calculated, and the simulated values of NOx concentration are compared with the measured values. The results are shown in Figure 8. It can be seen from Figure 8 that the relative errors between the calculated values and the measured values of the NOx concentration at the economizer outlet do not exceed 3.3% under different loads, which further proves the accuracy and reliability of the models established. It can also be seen from Figure 8 that the NOx concentration at the economizer outlet decreases first and then increases with the decrease in boiler load. When the boiler load is gradually reduced from 600 to 400 MW, the furnace center temperature will be reduced from 1678 K to 1423 K (see Figure 5). According to the calculation analysis the amount of thermal NOx formed is reduced by 13.26%, so the overall NOx concentration in the furnace is reduced. However, when the boiler load is reduced from 400 MW to 250 MW due to the increase in air–coal ratio in furnace, the $O_2$ concentration in the furnace increases, which results in an increase in fuel NOx so the NOx concentration increases to 392 mg/m$^3$.

As is shown in Figure 9, the variation trend of NOx concentration with the furnace height is basically the same. In the dry bottom hopper area the NOx concentration rises with the increase in furnace height, but due to the low temperature and the low oxygen content in the dry bottom hopper area, the NOx concentration in this area under different loads is lower than 324 mg/m$^3$. In the main combustion zone most of the pulverized coal burns here and a large amount of NOx is generated, which results in an overall increase in NOx concentration with the increase in furnace height. The NOx concentration in the main combustion zone increases by 39–51 mg/m$^3$ at different loads. Since the excess air coefficient in the burner zone is less than 1, some of the generated NOx is reduced by

the intermediates (such as CO). The concentration of NOx fluctuates at the height of each burner nozzle, and the fluctuation of NOx concentration is more obvious, especially at low loads.
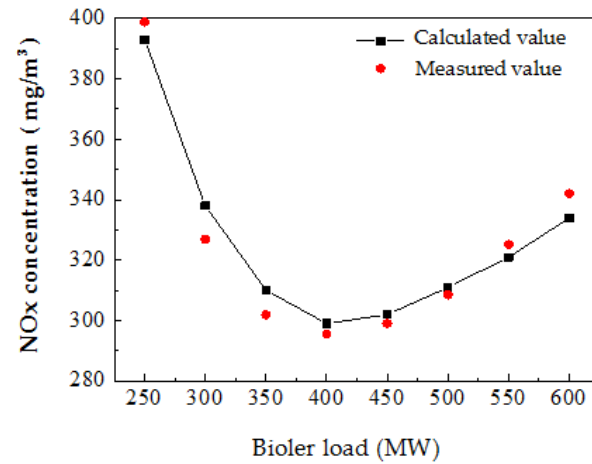


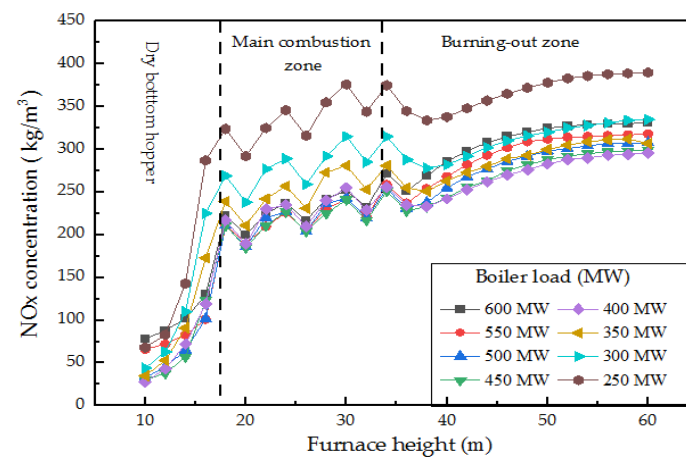**Figure 8.** Variation in NOx concentration with boiler loads.



**Figure 9.** Variation in NOx concentration along the furnace height under different boiler loads.

When operating at the boiler loads of 600 and 550 MW the six-layer burners are all put into operation, so the NOx concentration in the combustion zone increases more evenly when the flue gas flows upwards. When the boiler is operated under 500 and 450 MW loads the F-layer burners are turned off and the amount of pulverized coal injected into the furnace decreases, but there is still a small amount of air injected to the furnace through the burners out of operation and the oxidizing atmosphere is enhanced, which is conducive to the oxidation of intermediate products such as HCN and $NH_3$ from the middle and lower burners to generate NOx. Hence, there is still a large amount of NOx generated at the upper-layer burner position. When the boiler operates at 400 MW and below-400 MW loads the upper burners are all out of operation, so the fuel NOx generation is less in this area. Due to the low temperature in the center of the furnace in this area the thermal NOx is hardly generated, but the NOx concentration increases obviously with the increase in height in the middle and lower layer burner region. In the OFA area, the generated NOx is diluted by a large amount of OFA, so the NOx concentration at the height of OFA layer decreases by 20–41 mg/m$^3$. The amount of oxygen in the furnace is replenished in the area above the OFA nozzles, so the intermediates such as HCN and $NH_3$ from the combustion zone are oxidized to NOx. Therefore, with the increase in furnace height the concentration of NOx increases by 15–60 mg/m$^3$. In the area above the furnace arch the formation and reduction in NOx in the furnace tends to be balanced, and the NOx concentration is basically stable.

### 3.3. Effects of Air Amount on NOx Formation

In this section, under the boiler loads of 600, 500, 400 and 250 MW, the excess air coefficient, the OFA ratio, the primary air ratio and the internal secondary air ratio in the burner are changed in turn, and the furnace combustion and the NOx generation process are numerically simulated under different air distribution modes.

#### 3.3.1. Effects of Excess Air Coefficient

According to the actual operating conditions, the numerical simulation of changing the excess air coefficient is carried out under the load of 600, 500, 400 and 250 MW, respectively. The excess air coefficient is adjusted to 1.1, 1.2, 1.3, 1.4 and 1.5 when the coal feeding rate, the air distribution mode and the air distribution temperature of the boiler are kept unchanged. There are 20 operational conditions in total.

#### Effects of Excess Air Coefficient on NOx Concentration at Economizer Outlet

When the boiler is operated under different loads, Figure 10 shows the variation in NOx concentration at the economizer outlet with the excess air coefficient. It can be seen from Figure 10 that in the load range of 400–600 MW the NOx concentration at the economizer outlet goes up with the increase in the excess air coefficient. The reason is that a large amount of fuel NOx is generated because the increase in the air amount enhances the oxidizing atmosphere in the furnace. Under the high boiler loads, the variation amplitude of NOx with the excess air coefficient is also larger. Under the boiler load of 400, 500 and 600 MW, the NOx concentration at the economizer outlet increases by 53, 65 and 78 mg/m$^3$, respectively, when the excess air coefficient increases from 1 to 1.5. In addition, under the same load, when the excess air coefficient is larger the variation in NOx concentration with the excess air coefficient is smaller. This is because the increase in air volume reduces the early combustion temperature of pulverized coal and delays the combustion of pulverized coal, which finally reduces the thermal NOx production. At the boiler load of 250 MW, when the excess air coefficient is in the range of 1.3–1.5, the NOx concentration at the outlet of the economizer rises slightly with the increase in the excess air coefficient. However, when the excess air coefficient is less than 1.3 the NOx concentration increases as the excess air coefficient decreases. The reason is that the secondary air is mixed with the pulverized coal prematurely due to the small amount of primary air at the outlet of a single burner, which results in a large amount of NOx at the outlet of the burner.
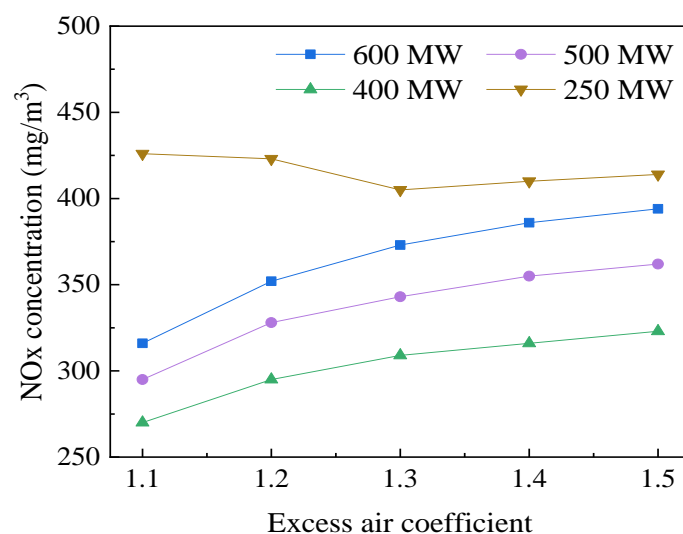


**Figure 10.** Variation in NOx concentration with excess air coefficient at the economizer outlet.

Effects of Excess Air Coefficient on NOx Distribution in the Furnace

Under the different excess air coefficient, the variation curves of NOx concentration along the furnace height are shown in Figure 11. Figure 11a–d separately corresponds to four different boiler loads. It can be seen from Figure 11 that the NOx concentration in the furnace increases with the increase in furnace height on the whole, corresponding to each excess air coefficient under four different boiler loads. When the excess air coefficient is larger, the NOx concentration fluctuates greatly in the main combustion zone. At the nozzle height of the burning-out zone, the NOx concentration decreases because NOx is diluted by the OFA injected. In the area above the OFA nozzle the NOx concentration rises slowly with the increase in furnace height owing to the good oxidizing atmosphere, and finally tends to be stable. When the excess air coefficient is larger, the NOx concentration in the burning-out zone increases greatly.
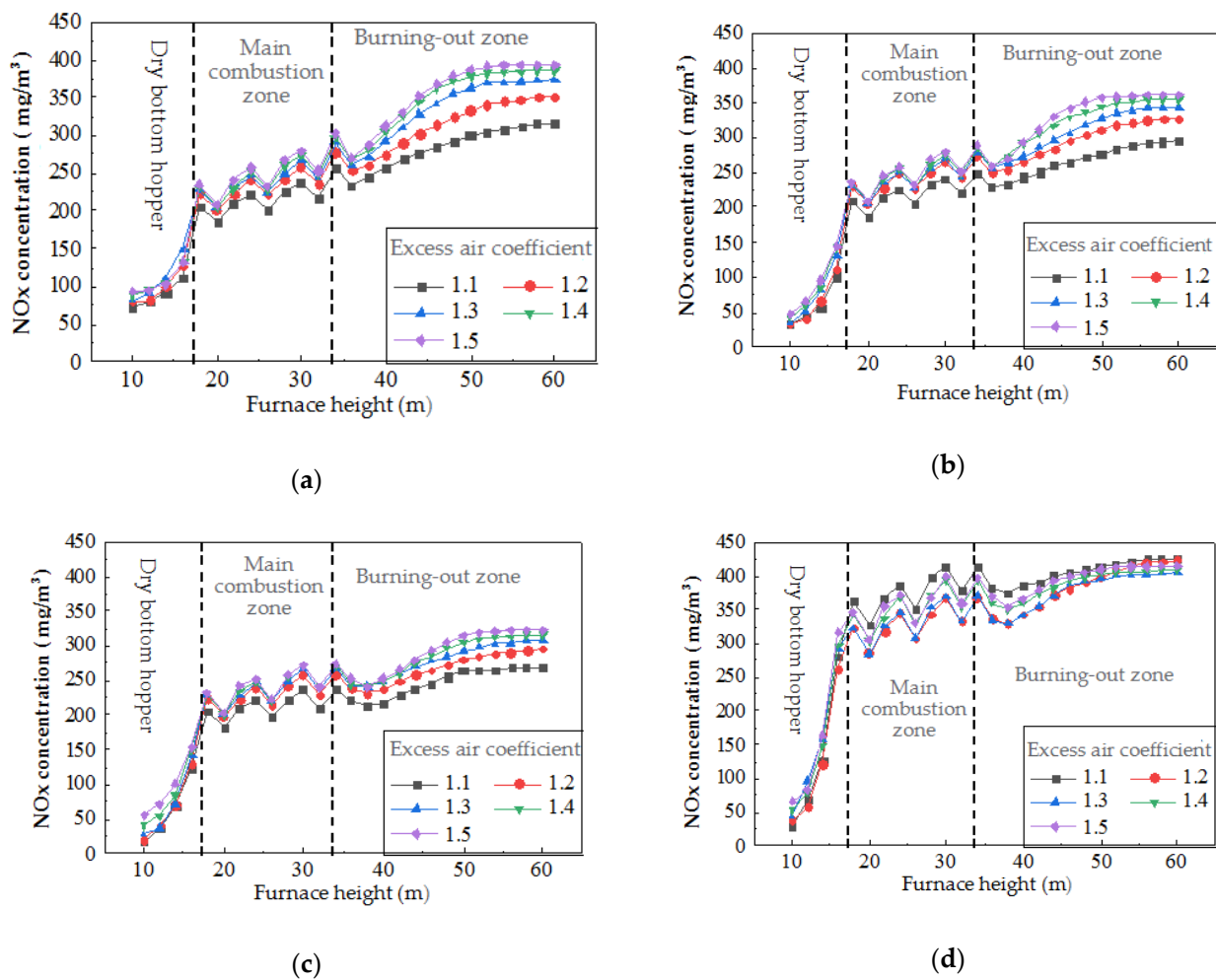


**Figure 11.** Variation in NOx concentration along the furnace height under different excess air coefficient: (**a**) Variation in NOx concentration along furnace height under different excess air coefficient and 600 MW boiler load; (**b**) Variation in NOx concentration along the furnace height under different excess air coefficient and 500 MW boiler load; (**c**) Variation in NOx concentration along the furnace height under different excess air coefficient and 400 MW boiler load; (**d**) Variation in NOx concentration along the furnace height under different excess air coefficient and 250 MW boiler load.

### 3.3.2. Effects of OFA Ratio

The effect of OFA ratio on NOx is that it reduces the amount of oxygen in the main combustion zone and makes the pulverized coal burn in stages in the main combustion zone and the burning-out zone. The air staged combustion can effectively reduce the NOx formation during coal combustion. In this section, under the boiler load of 600, 500, 400 and 250 MW, respectively, the total air amount and the air distribution temperature are kept unchanged and the OFA ratio is set as 15%, 20%, 25%, 30% and 35%, respectively. The numerical simulations of different OFA ratios are carried out, there being a total of 20 working conditions.

Effects of OFA Ratio on NOx Concentration at Economizer Outlet

Under different boiler loads, the variation in NOx concentration at the economizer outlet with the OFA ratio is shown in Figure 12. It can be seen from Figure 12 that the NOx concentration at the economizer outlet decreases with the increase in the OFA ratio. This is because the increase in the OFA ratio can enhance the air staging effect and reduce the oxygen content in the combustion zone, which can inhibit the formation of NOx. At the boiler loads of 600, 500, 400 and 250 MW, when the OFA ratio is increased from 15% to 35%, the NOx concentration at the economizer outlet decreases by 36, 41, 46 and 57 mg/m$^3$, respectively. This indicates that the variation in NOx concentration with the OFA ratio is more obvious under the low boiler load. The reason is that the NOx generated in the furnace under the low boiler load is almost the fuel NOx, which is more sensitive to the oxygen content.
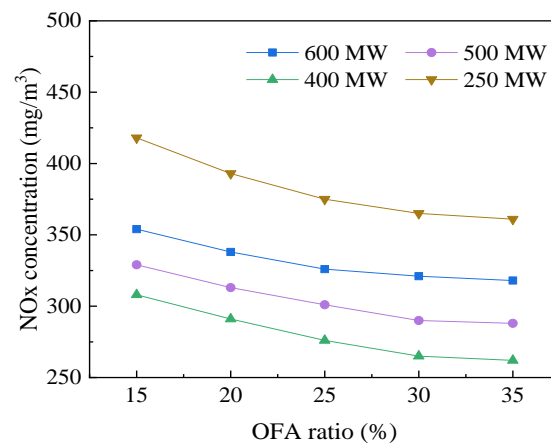


**Figure 12.** Variation in NOx concentration at economizer outlet with the OFA ratio.

Effects of OFA Ratio on NOx Distribution in the Furnace

The curves of NOx concentration varying with the furnace height are illustrated in Figure 13 under different OFA ratios. Figure 13a–d separately corresponds to four different boiler loads. It can be seen from Figure 13 that the NOx concentration in the furnace increases with the increase in furnace height on the whole, corresponding to each OFA ratio under four different boiler loads. When the OFA ratio is larger the increase in NOx concentration in the main combustion zone is smaller, meanwhile the air amount in the main combustion zone is small and the fluctuation of NOx concentration in this zone is small. In the area above the OFA nozzles the NOx concentration goes up with the increase in furnace height, and when the OFA ratio is larger the increase in NOx concentration is also larger.
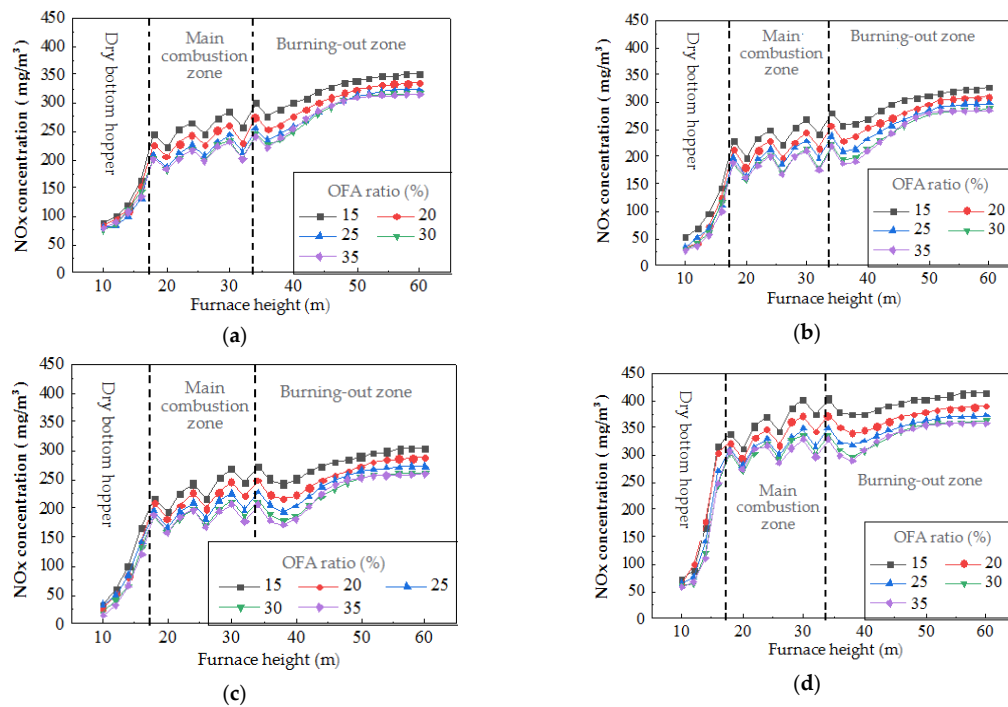
**Figure 13.** Variation in NOx concentration along the furnace height under different OFA ratios: (**a**) Variation in NOx concentration along the furnace height under different OFA ratio and 600 MW boiler load; (**b**) Variation in NOx concentration along the furnace height under different OFA ratio and 500 MW boiler load; (**c**) Variation in NOx concentration along the furnace height under different OFA ratio and 400 MW boiler load; (**d**) Variation in NOx concentration along the furnace height under different OFA ratio and 250 MW boiler load.

### 3.3.3. Effects of Primary Air Ratio

The change in primary air ratio can affect the flow field, the temperature field and the combustion process of pulverized coal at the outlet of the burner. In this section, under the boiler load of 600, 500, 400 and 250 MW, respectively, keeping the total air amount and the air temperature unchanged the primary air ratio is adjusted to 20%, 22.5%, 25%, 27.5% and 30%, respectively. The numerical simulations of operating conditions at four primary air ratios are implemented, there being 20 working conditions in total.

Effects of Primary Air Ratio on NOx Concentration at Economizer Outlet

When the boiler operates under different loads, the variation in NOx concentration at the economizer outlet with the primary air ratio is shown in Figure 14. It can be seen from Figure 14 that the NOx concentration at the economizer outlet increases with the increase in the primary air ratio in the range of 400–600 MW load, and the NOx concentration varies greatly with the primary air ratio under high boiler loads. The reason is that a large amount of NOx is generated at the initial stage of combustion because the air–coal ratio at the outlet of the burner increases and the oxidizing atmosphere is enhanced with increasing the primary air ratio. Additionally, the amount of CO is reduced owing to the increase in $O_2$ content, so the reduction in NOx by CO is weakened, which can contribute to NOx formation. At the boiler loads of 400, 500 and 600 MW, when the primary air ratio increases from 20% to 30%, the NOx concentration at the economizer outlet increases by 36, 42 and 49 mg/m$^3$, respectively. Under the boiler load of 250 MW, when the primary air ratio is raised from 22.5% to 30% the NOx concentration at the economizer outlet rises slightly. However, when the primary air ratio is less than 22.5% a large amount of fuel-type NOx is generated because of the advance ignition of pulverized coal. Hence, the NOx concentration is reduced by means of increasing the primary air ratio to delay the ignition of pulverized coal.
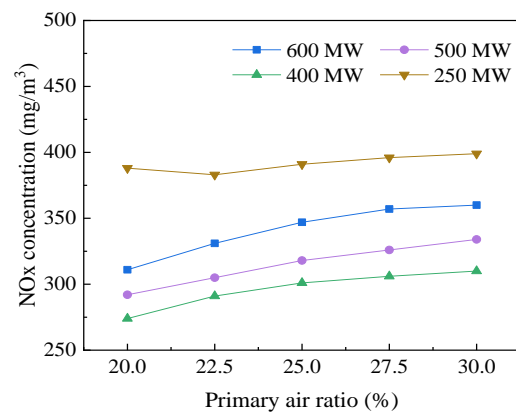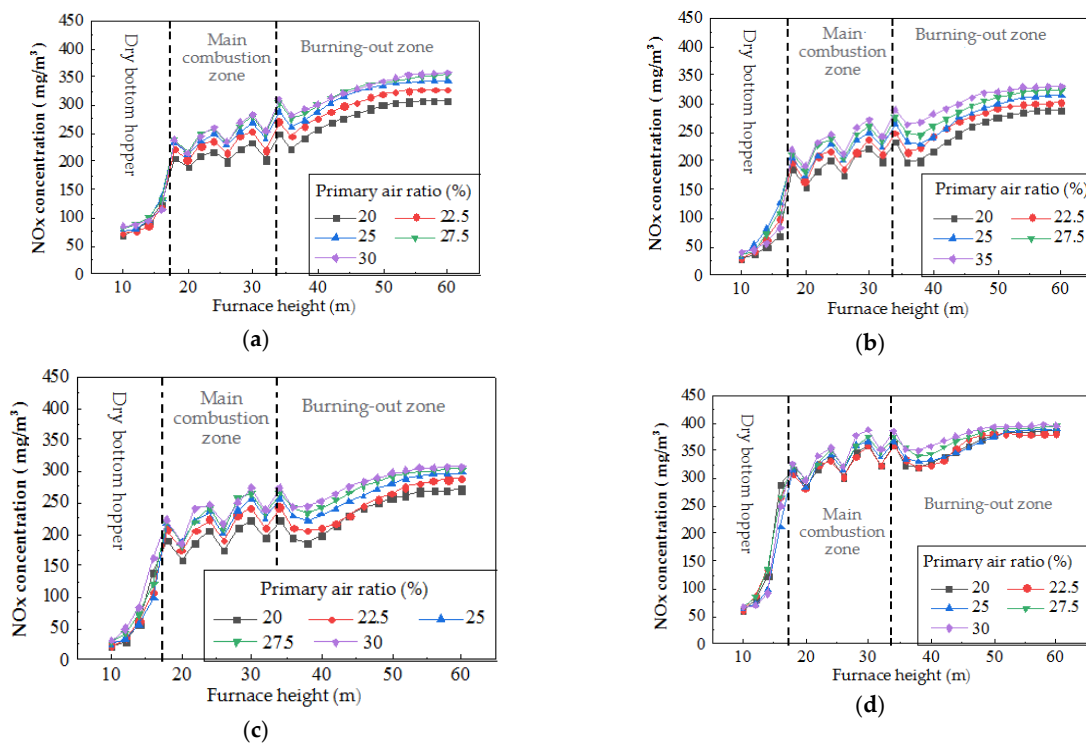
**Figure 14.** Variation in NOx concentration at economizer outlet with the primary air ratio.

Effects of Primary Air Ratio on NOx Distribution in Furnace

Under the boiler loads of 600, 500, 400 and 250 MW, when the primary air ratio is different, the variation curves of NOx concentration with the furnace height are illustrated in Figure 15a–d. It can be seen that under different operating conditions the NOx concentration in the main combustion zone increases with the increase in furnace height as a whole. When the primary air ratio is larger the increase in NOx concentration is larger, and the fluctuation of NOx concentration in this area is also larger. In the zone above the OFA nozzles the NOx concentration rises with the furnace height increasing, and when the primary air ratio is small the increase in NOx concentration in the burning-out zone is large.



**Figure 15.** Variation in NOx concentration along the furnace height under different primary air ratio: (**a**) Variation in NOx concentration along the furnace height under different primary air ratio and 600 MW boiler load; (**b**) Variation in NOx concentration along the furnace height under different primary air ratio and 500 MW boiler load; (**c**) Variation in NOx concentration along the furnace height under different primary air ratio and 400 MW boiler load; (**d**) Variation in NOx concentration along the furnace height under different primary air ratio and 250 MW boiler load.

### 3.3.4. Effects of Internal Secondary Air Ratio

In this study, the ratio of the internal secondary air to the external secondary air of the burners can be adjusted, which can affect the pulverized coal combustion and the NOx generation. When the internal secondary air ratio is small the recirculation zone is small, which weakens the ability to entrain the high-temperature flue gas. In order to study the influence of internal secondary air on NOx generation under the boiler load of 600, 500, 400 and 250 MW, respectively, and keeping the total air amount and the air temperature unchanged, the numerical simulation calculation has been performed when the internal secondary air ratio is set as 20%, 27.5%, 35%, 42.5% and 50%, respectively. There are 20 working conditions simulated in total.

Effects of Internal Secondary Air Ratio on NOx Concentration at Economizer Outlet

The variation in NOx concentration at the economizer outlet with the internal secondary air ratio when the boiler operates under different loads is shown in Figure 16. It can be seen from Figure 16 that the NOx concentration at the economizer outlet decreases first and then increases with the increase in the internal secondary air ratio under four boiler loads, and the NOx concentration varies greatly with the internal secondary air ratio under low boiler loads. When the internal secondary air ratio is small the increase in the internal secondary air amount can enlarge the internal recirculation zone at the outlet of the burners, which delays the mixing of the pulverized coal–air flow and the secondary air and strengthens the combustion classification effect, so the formation of fuel NOx is inhibited. When the internal secondary air ratio is large, the amount of high temperature flue gas entrained by the internal secondary air increases, which enhances the initial stage temperature of the pulverized coal combustion and then increases the amount of thermal NOx generation. In addition, the increment of thermal NOx is greater than the reduction in fuel NOx. Therefore, the NOx concentration at the economizer outlet decreases first and then increases with the increase in the internal secondary air ratio. When the boiler load is low the combustion aerodynamic field is unstable due to the small primary air rate and the small secondary air rate at the burner outlet, so the formation of NOx is more affected by the internal secondary air ratio. At the boiler load of 400 MW, when the internal secondary air ratio is 35%, the minimum NOx emission at the economizer outlet is 280 mg/m$^3$.
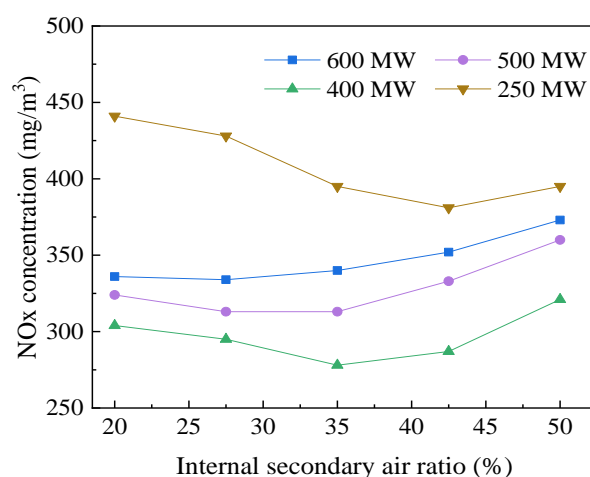


**Figure 16.** Variation in NOx concentration at economizer outlet with the internal secondary air ratio.

Effects of Internal Secondary Air Ratio on NOx Distribution in Furnace

At the boiler loads of 600, 500, 400 and 250 MW, respectively, when the internal secondary air ratio is different the variation curves of NOx concentration with furnace height are shown in Figure 17. It can be seen from this figure that the trends of NOx concentration changing with furnace height are basically the same under different working conditions. Due to the low temperature and the low oxygen content in the cold hopper area, the NOx

concentration is less than 330 mg/m$^3$. In the combustion zone and the burning-out zone, with the increase in the supply air rate in the furnace a large amount of NOx is generated. However, from the position of 5 m above the OFA the NOx concentration is basically no longer changed, because the air rate is no longer provided in the furnace and the pulverized coal combustion reaction is also completed. In the main combustion zone, when the internal secondary air ratio varies the increased amplitude of NOx concentration changes with the increase in furnace height, while the increased amplitude of NOx concentration in the burning-out zone is basically unchanged; this indicates the influence of internal secondary air on NOx formation that mainly occurs in the main combustion zone.
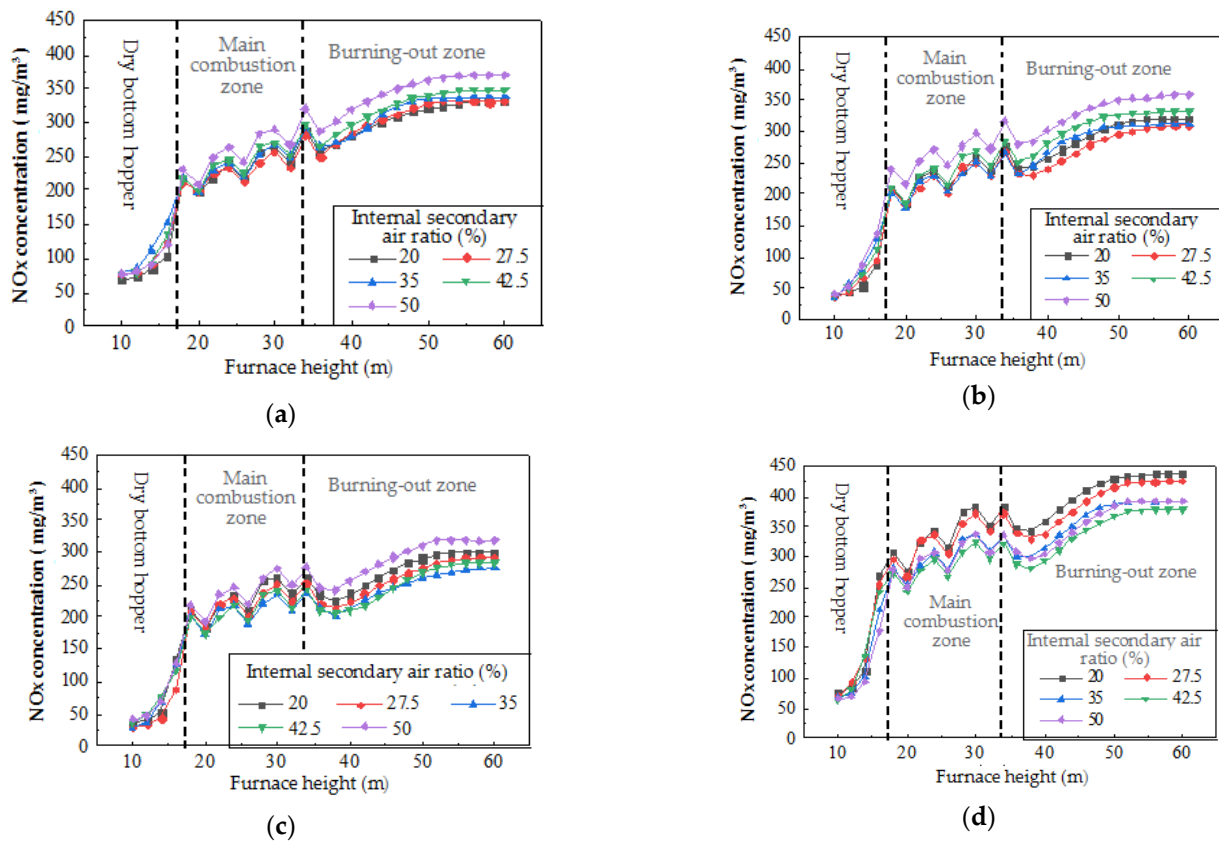


**Figure 17.** Variation in NOx concentration along the furnace height under different internal secondary air ratio: (**a**) Variation in NOx concentration along the furnace height under different internal secondary air ratio and 600 MW boiler load; (**b**) Variation in NOx concentration along the furnace height under different internal secondary air ratio and 500 MW boiler load; (**c**) Variation in NOx concentration along the furnace height under different internal secondary air ratio and 400 MW boiler load; (**d**) Variation in NOx concentration along the furnace height under different internal secondary air ratio and 250 MW boiler load.

### 3.4. Effects of Supply Air Temperature on NOx Formation

The temperature increase in the supply air can raise the overall temperature in the furnace and make the pulverized coal catch fire in advance, which can affect the formation and the reduction in NOx. To study the effects of supply air temperature on NOx when the primary and secondary air temperatures are changed in turn under the boiler loads of 600, 500, 400 and 250 MW, the combustion and NOx formation processes in the furnace are numerically simulated and analyzed.

3.4.1. Effects of Primary Air Temperature on NOx Concentration at Economizer Outlet

According to the actual operating conditions under the boiler load of 600, 500, 400 and 250 MW, respectively, and keeping the total air amount and the air distribution mode

unchanged, the numerical simulation calculation has been carried out when the primary air temperature is set as 335 K, 345 K, 355 K, 365 K and 375 K. There are a total of 20 working conditions.

The variation curves of NOx concentration at the economizer outlet with the primary air temperature under different boiler loads are shown in Figure 18. It can be seen from the figure that the NOx concentration at the economizer outlet increases when the primary air temperature goes up, and the NOx concentration varies more obviously with the primary air temperature under high boiler load. When increasing the primary air temperature the overall temperature level in furnace increases. Consequently, the thermal NOx increases exponentially, and the fuel NOx generation also increases because the pulverized coal burns ahead of schedule and a large number of volatiles are released. This is why the NOx concentration at the economizer outlet increases. The thermal NOx accounts for a large proportion under high boiler load and the thermal NOx is more affected by the primary air temperature, so the NOx concentration varies more. When the primary air temperature is increased from 335 K to 375 K the NOx concentration at the economizer outlet increases by 55, 33, 22, and 10 mg/m$^3$ at the boiler load of 600, 500, 400 and 250 MW, respectively.
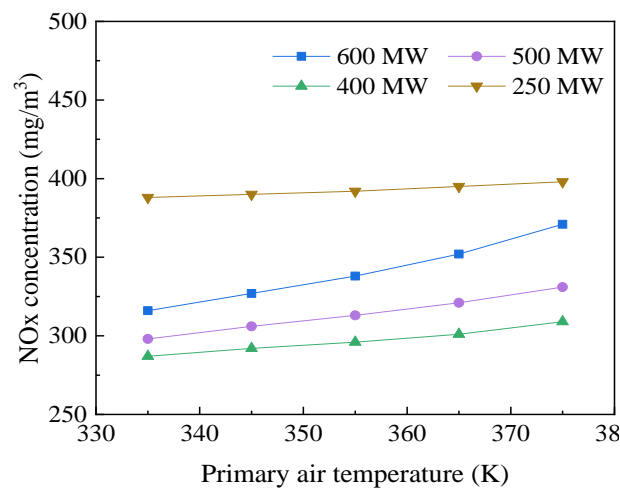


**Figure 18.** Variation in NOx concentration at economizer outlet with the primary air temperature.

3.4.2. Effects of the Temperature of Secondary Air and OFA on NOx Concentration at Economizer Outlet

The proportion of the secondary air and the OFA accounting for the total air amount is larger, hence their temperature change can influence the overall temperature field in the furnace, and then the NOx generation. According to the actual operating conditions, under the boiler loads of 600, 500, 400 and 250 MW, respectively, and keeping the total air amount and the air distribution mode unchanged, the numerical simulation calculation has been carried out when the temperature of secondary air and OFA is set as 550 K, 555 K, 560 K, 565 K and 570 K. There are a total of 20 working conditions.

The variation curves of NOx concentration at the economizer outlet with the temperature of secondary air and OFA under different boiler loads are shown in Figure 19. It can be seen from the figure that the NOx concentration at the economizer outlet increases when the temperature of secondary air and OFA rises. In addition, the concentration of NOx varies more obviously with the temperature of secondary air and OFA under high boiler load. When raising the temperature of secondary air and OFA, the overall temperature level in the furnace increases, which leads to the increase in NOx generation. When the temperature of secondary air and OFA is raised from 550 K to 570 K the NOx concentration at the economizer outlet increases by 83, 53, 30, and 14 mg/m$^3$ at the boiler loads of 600, 500, 400 and 250 MW, respectively. The above data show that the influence of the temperature change in secondary air and OFA is greater than that of the primary air temperature change.
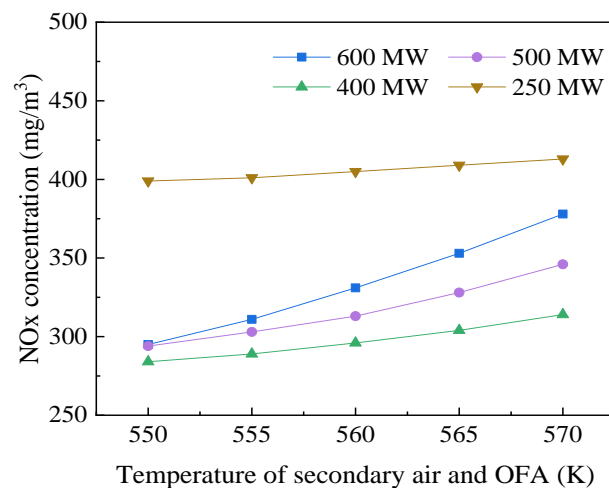
**Figure 19.** Variation in NOx concentration at economizer outlet with the temperature of secondary air and OFA.

## 4. Conclusions

In this work, taking a 600 MW supercritical opposed firing pulverized coal boiler as the research object, the numerical simulation models of pulverized coal combustion and a full-scale three-dimensional physical model of the boiler are established, which are the basis of the simulation research. The simulation data of the base operating conditions are compared with the field test data, which has verified the accuracy and the reliability of the models established. On that basis, the combustion numerical simulation of 128 groups of variable working conditions has been performed. The effects of boiler load, the air rate and the air temperature on the formation and the distribution of NOx in the furnace have been emphatically analyzed.

The simulation results show the NOx concentration goes up with the increase in furnace height when all the parameters discussed are changed, until it tends towards stability in the burning-out zone. However, the NOx concentration is low in the dry bottom hopper, and it fluctuates greatly in the main combustion zone. When the boiler load is reduced from 600 to 250 MW, the NOx concentration at the economizer outlet decreases first and then increases. When the boiler runs at medium and high loads, the increase in excess air coefficient can enhance the NOx concentration at the economizer outlet because of generating much fuel NOx. However, when the excess air coefficient is less than 1.3, the NOx concentration at the economizer outlet increases as the excess air coefficient decreases under the load of 250 MW. Owing to its air staging effect, the increase in OFA ratio not only reduces the NOx concentration at the economizer outlet, but also improves the combustion stability of the boiler. With the decrease in boiler load, the effect of the OFA ratio on NOx concentration at the economizer outlet increases gradually. The increase in primary air can raise the NOx concentration at the economizer outlet at medium and high boiler loads because of the enhanced oxidizing atmosphere in the furnace. The NOx concentration at the economizer outlet decreases first and then increases with the increase in the internal secondary air ratio; especially, the NOx concentration varies greatly under low boiler loads. The above analyses indicate that the effects of the air rate and air distribution on the NOx formation are very different under variable working conditions. Additionally, the temperature increases in the primary air, the secondary air, and the OFA all lead to the increase in NOx concentration in the furnace, and the influence of the secondary air temperature and the OFA temperature is greater than that of the primary air temperature. Compared with the burning-out zone, the air temperature has a greater influence on NOx formation in the main combustion zone. At high boiler load, the NOx concentration is more affected by the air temperature.

The pulverized coal combustion and NOx formation in the furnace involve the physical and chemical processes, including a series of parallel and continuous reactions, homogeneous and heterogeneous reactions, free radical reactions and molecular reactions. Hence, they are extremely complex and are simultaneously influenced by many factors in the actual operation, and these factors often interact with each other. Their complex characteristics make the experimental research a challenging task, especially under large quantities of variable operating conditions. The experimental research of pulverized coal combustion and NOx formation is usually restricted by many field operational requirements. The numerical simulation of the pulverized coal combustion and NOx formation based on Fluent Software can provide a lot of detailed information in order to obtain the optimum operating conditions and the optimum control strategy. Furthermore, large amounts of simulation data are a new data source for further research on the NOx prediction model at the economizer outlet. It can improve the prediction ability and the generalization ability of the NOx prediction model.

## References

1. Zhang, Z.; Song, G.; Chen, C.; Han, Z. Cause analysis of ammonia escape in SCR flue gas denitrification process for 600 MW units. *Electr. Power Constr.* **2012**, *33*, 67–70.
2. Liu, T. Analysis on measurement and control strategy for denitration system of thermal power generating units and its optimization. *Zhejiang Electr. Power* **2016**, *35*, 42–44.
3. Chang, J.; Zhou, Z.; Ma, X.; Liu, J. Computational investigation of hydrodynamics, coal combustion and NOx emissions in a tangentially fired pulverized coal boiler at various loads. *Particuology* **2022**, *65*, 105–116. [CrossRef]
4. Yuan, L. Numerical Simulation of Variable Load Combustion of Supercritical Pulverized Coal Boiler and Optimization of Air Distribution. Master's Thesis, Southeast University, Nanjing, China, 2019.
5. Wang, Y.; Zhou, Y. Numerical optimization of the influence of multiple deep air-staged combustion on the NOx emission in an opposed firing utility boiler using lean coal. *Fuel* **2020**, *269*, 116996. [CrossRef]
6. Zeinivand, H.; Bazdidi-Tehrani, F. Influence of stabilizer jets on combustion characteristics and NOx emission in a jet-stabilized combustor. *Appl. Energy* **2012**, *92*, 348–360. [CrossRef]
7. Shameer, P.M.; Ramesh, K. Experimental evaluation on performance, combustion behavior and influence of in-cylinder temperature on NOx emission in a DI diesel engine using thermal imager for various alternate fuel blends. *Energy* **2017**, *118*, 1334–1344. [CrossRef]
8. Hayhurst, A.N.; Vince, I.M. Nitric oxide formation from $N_2$ in flames: The importance of "prompt" NO. *PECS* **1980**, *6*, 35–51. [CrossRef]
9. Glarborg, P.; Jensen, A.D.; Johnson, J.E. Fuel nitrogen conversion in solid fuel fired systems. *PECS* **2003**, *29*, 89–113. [CrossRef]
10. Zeldvich, Y.B. The oxidation of nitrogen in combustion and explosions. *J. Acta Physicochim.* **1946**, *21*, 577.
11. De Soete, G.G. Overall reaction rates of NO and $N_2$ formation from fuel nitrogen. *Symp. Combust.* **1975**, *15*, 1093–1102. [CrossRef]
12. Wang, L.; Miao, Z.; Li, J.; Huang, W.; Peng, B. Research on reduced-NOx simulation and wall-type OFA-NOx formation mechanism of 600 MW pulverized coal boiler. *Boil. Technol.* **2014**, *45*, 49–52. [CrossRef]
13. Fenimore, C.P. Studies of fuel-nitrogen species in rich flame gases. *Symp. Combust.* **1979**, *17*, 661–670. [CrossRef]

14. Li, J.; Brzdekiewicz, A.; Yang, W.; Blasiak, W. Co-firing based on biomass torrefaction in a pulverized coal boiler with aim of 100% fuel switching. *Appl. Energy* **2012**, *99*, 344–354. [CrossRef]
15. Ma, L.; Fang, Q.; Yin, C.; Wang, H.; Zhang, C.; Chen, G. Novel corner-fired boiler system of improved efficiency and coal flexibility and reduced NOx emissions. *Appl. Energy* **2019**, *238*, 453–465. [CrossRef]
16. Zhao, S.; Fang, Q.; Yin, C.; Wei, T.; Wang, H.; Zhang, C.; Chen, G. New fuel air control strategy for reducing NOx emissions from corner-fired utility boilers at medium-low loads. *Energy Fuels* **2017**, *31*, 6689–6699. [CrossRef]
17. Choi, C.R.; Kim, C.N. Numerical investigation on the flow, combustion and NOx emission characteristics in a 500 MWe tangentially fired pulverized-coal boiler. *Fuel* **2009**, *88*, 1720–1731. [CrossRef]
18. Jiang, Y.; Jeon, C.H. Comparative study on combustion and emission characteristics of torrefied and ashless biomass with coal through the 500 MW tangentially fired boiler simulation. *Energy Fuels* **2021**, *35*, 561–574. [CrossRef]
19. Fortunato, V.; Galletti, C.; Tognotti, L.; Parente, A. Influence of modelling and scenario uncertainties on the numerical simulation of a semi-industrial flameless furnace. *Appl. Therm. Eng.* **2015**, *76*, 324–334. [CrossRef]
20. Li, Z.; Zhang, Z.; Chen, D.; Parente, A. Prediction of NOx during pulverized coal combustion: Model development and its implementation with fluent. *J. China Coal Soc.* **2016**, *41*, 2426–2433.
21. Tan, P. Modeling and Optimization of the Combustion Characteristics in Low NOx Combustion Pulverized Coal-Fired Boilers under Coal Blending Conditions. Ph.D. Thesis, Huazhong University of Science & Technology, Wuhan, China, 2017.
22. Perry, S.T.; Fletcher, T.H.; Solum, M.S.; Pugmire, R.J. Modeling nitrogen evolution during coal pyrolysis based on a global free-radical mechanism. *Energy Fuels* **2000**, *14*, 1094–1102. [CrossRef]
23. Genetti, D.; Fletcher, T.H. Modeling nitrogen release during devolatilization on the basis of chemical structure of coal. *Energy Fuels* **1999**, *13*, 1082–1091. [CrossRef]
24. Zhang, Y. Numerical simulation of gas solid flow and NOx generation in a new type of dual circulating fluidized bed boiler. Master's Thesis, Chongqing University, Chongqing, China, 2017.
25. Lamioni, R.; Bronzoni, C.; Folli, M.; Tognotti, L.; Galletti, C. Feeding $H_2$-admixtures to domestic condensing boilers: Numerical simulations of combustion and pollutant formation in multi-hole burners. *Appl. Energy* **2022**, *309*, 118379. [CrossRef]
26. Kim, B.S.; Kim, T.Y.; Park, T.C.; Yeo, Y.K. Comparative study of estimation methods of NOx emission with selection of input parameters for a coal-fired boiler. *Korean J. Chem. Eng.* **2018**, *35*, 1779–1790. [CrossRef]
27. Shi, Y.; Zhong, W.; Chen, X.; Yu, A.B.; Li, J. Combustion optimization of ultra-supercritical boiler based on artificial intelligence. *Energy* **2019**, *170*, 804–817. [CrossRef]
28. Ye, T.; Dong, M.; Liang, Y.; Long, J.; Li, W.; Lu, J. Modeling and optimization of the NOX generation characteristics of the coal-fired boiler based on interpretable machine learning algorithm. *Int. J. Green Energy* **2022**, *19*, 529–543. [CrossRef]
29. Zhao, L.; Zhou, Q.; Zhao, C. Flame characteristics in a novel petal swirl burner. *Combust. Flame* **2008**, *155*, 277–288. [CrossRef]
30. Shang, B. Research on NOx Prediction Model of Economizer Outlet of 600MW Coal-Fired Unit Based on Numerical Simulation. Master's Thesis, Southeast University, Nanjing, China, 2022.
31. Li, X. Numerical simulation of coal combustion in a 1000MW ultra-supercritical opposed swirling fired utility Boiler. Master's Thesis, Huazhong University of Science & Technology, Wuhan, China, 2012.
32. Bai, T. Numerical Simulation and Experimental Investigation on Low-NOx Combustion System in Pulverized Coal Boiler. Ph.D. Thesis, North China Electric Power University, Beijing, China, 2014.
33. Gosman, A.D.; Loannides, E. Aspects of computer simulation of liquid-fueled combustors. *J. Energy* **1983**, *7*, 482–490. [CrossRef]
34. Lu, B. Numerical Simulation of Combustion and NOx Emission in a Purely High Alkali Coal Fired Boiler. Master's Thesis, North China Electric Power University, Beijing, China, 2018.
35. Liu, H.; Liu, Y.; Yi, G.; Nie, L.; Che, D. Effects of air staging conditions on the combustion and NOx mission characteristics in a 600 MW wall fired utility boiler using lean coal. *Energy Fuels* **2013**, *27*, 5831–5840. [CrossRef]
36. Drosatos, P.; Nikolopoulos, N.; Nikolopoulos, A.; Papapavlou, C.; Grammelis, P.; Kakaras, E. Numerical examination of an operationally flexible lignite-fired boiler including its convective section using as supporting fuel pre-dried lignite. *Fuel Process. Technol.* **2017**, *166*, 237–257. [CrossRef]
37. Hill, S.C.; Smoot, L.D. Modeling of nitrogen oxides formation and destruction in combustion systems. *Prog. Energy Combust. Sci.* **2000**, *26*, 417–458. [CrossRef]
38. Pallarés, J.; Gil, A.; Cortés, C.; Herce, C. Numerical study of co-firing coal and Cynara cardunculus in a 350 MWe utility boiler. *Fuel Process. Technol.* **2009**, *90*, 1207–1213. [CrossRef]
39. Zhou, H.; Mo, G.; Si, D.; Cen, K. Numerical simulation of the NO x emissions in a 1000 MW tangentially fired pulverized-coal boiler: Influence of the multi-group arrangement of the separated over fire air. *Energy Fuels* **2011**, *25*, 2004–2012. [CrossRef]
40. Diez, L.I.; Cortés, C.; Pallarés, J. Numerical investigation of NOx emissions from a tangentially-fired utility boiler under conventional and overfire air operation. *Fuel* **2008**, *87*, 1259–1269. [CrossRef]
41. Li, Z.; Miao, Z.; Shen, X.; Li, J. Effects of momentum ratio and velocity difference on combustion performance in lignite-fired pulverized boiler. *Energy* **2018**, *165*, 825–839. [CrossRef]
42. Sheng, C.; Moghtaderi, B.; Gupta, R.; Wall, T.F. A computational fluid dynamics based study of the combustion characteristics of coal blends in pulverized coal-fired furnace. *Fuel* **2004**, *83*, 1543–1552. [CrossRef]

43. Zha, Q.; Li, D.; Che, D. Numerical evaluation of heat transfer and NOx emissions under deep-air- staging conditions within a 600 MWe tangentially fired pulverized-coal boiler. *Appl. Therm. Eng.* **2017**, *116*, 170–181. [CrossRef]
44. Yi, Z.; Hu, X. Numerical simulation of by-product fuel combustion in a tangential gas-fired boiler: Effect of proportion and angle on coke oven gas. *J. Energy Eng.* **2022**, *148*, 04022006. [CrossRef]